Sequential defects in cardiac lineage commitment and maturation cause hypoplastic left heart syndrome

Markus Krane, MD[1,2†], Martina Dreßen, PhD[1†], Gianluca Santamaria, PhD[3†], Ilaria My, MD[3†], Christine M. Schneider, MD[3†], Tatjana Dorn, PhD[3†], Svenja Laue, PhD[3†], Elisa Mastantuono, MD[3,4], Riccardo Berutti, PhD[4], Hilansi Rawat, MS[3], Ralf Gilsbach, PhD[5,6,7], Pedro Schneider, MD[5], Harald Lahm, PhD[1], Sascha Schwarz, MS[8], Stefanie A. Doppler, PhD[1], Sharon Paige, MD, PhD[9], Nazan Puluca, MD[1], Sophia Doll, PhD[10], Irina Neb, MS[1], Thomas Brade, PhD[3], Zhong Zhang[1], Claudia Abou-Ajram[1], Bernd Northoff, MS[11], Lesca M. Holdt, MD[11], Stefanie Sudhop, PhD[8], Makoto Sahara, MD[12], Alexander Goedel, MD[3], Andreas Dendorfer, MD[2,13], Fleur V.Y. Tjong, MD, PhD[14], Maria E. Rijlaarsdam, MD[15], Julie Cleuziou, MD[16], Nora Lang, MD[17], Christian Kupatt, MD[2,3], Connie Bezzina, MD[14], Rüdiger Lange, MD[1,2], Neil E. Bowles, PhD[18], Matthias Mann, PhD[10], Bruce Gelb, MD[19], Lia Crotti, MD[20,21,22], Lutz Hein, MD[5,23], Thomas Meitinger, PhD[2,4], Sean Wu, MD[9], Daniel Sinnecker, MD[2,3], Peter J. Gruber, MD, PhD[24]*, Karl-Ludwig Laugwitz, MD[2,3]*, and Alessandra Moretti, PhD[2,3]*

[1] Department of Cardiovascular Surgery, Institute Insure, German Heart Center Munich, Technical University of Munich, Lazarettstrasse 36, 80636 Munich, Germany

[2] DZHK (German Centre for Cardiovascular Research) - partner site Munich Heart Alliance, Munich, Germany

[3] First Department of Medicine, Cardiology, Klinikum rechts der Isar - Technical University of Munich, Ismaninger Straβe 22, 81675 Munich, Germany

[4] Institute of Human Genetics, Klinikum rechts der Isar - Technical University of Munich, Ismaninger Strasse 22, 81675 Munich, Germany, and Helmholtz Zentrum München, Ingolstaedter Landstraβe 1, 85764 Neuherberg, Germany

[5] Institute of Experimental and Clinical Pharmacology and Toxicology University of Freiburg Albertstrasse 25, 79104 Freiburg, Germany

[6] Institute for Cardiovascular Physiology, Goethe University, Frankfurt am Main, Germany

[7] DZHK (German Centre for Cardiovascular Research) - partner site RheinMain, Frankfurt am Main, Germany

[8] Center for Applied Tissue Engineering and Regenerative Medicine (CANTER), Munich University of Applied Sciences, Lothstr. 34, 80335 Munich, Germany

[9] Cardiovascular Institute, Stanford University School of Medicine, Stanford, CA 94305, USA

[10] Proteomics and Signal Transduction, Max-Planck Institute of Biochemistry, 82152 Martinsried, Germany

[11] Institute of Laboratory Medicine, University Hospital, LMU Munich, Marchioninistraβe 15, 81377 Munich, Germany.

[12] Department of Cell and Molecular Biology, Karolinska Institute, Stockholm 171 77, Sweden

[13] Walter-Brendel-Centre of Experimental Medicine, University Hospital, LMU Munich, Marchioninistr. 27, 81377 Munich, Germany

[14] Department of Clinical and Experimental Cardiology, Amsterdam UMC, University of Amsterdam, Heart Centre, 1105 AZ Amsterdam, The Netherlands

[15] Department of Pediatric Cardiology, Leiden University Medical Center, Leiden, The Netherlands

[16] Department of Congenital and Paediatric Heart Surgery, German Heart Center Munich, Technical University of Munich, Lazarettstrasse 36, 80636 Munich, Germany

[17] Department of Paediatric Cardiology and Congenital Heart Defects, German Heart Center Munich, Technical University of Munich, Lazarettstrasse 36, 80636 Munich, Germany

[18] Department of Pediatrics (Division of Cardiology), University of Utah School of Medicine, Salt Lake City, UT, USA

1   [19] The Mindich Child Health and Development Institute, Icahn School of Medicine at Mount Sinai, New
2   York, NY 10029, USA
3   [20] Istituto Auxologico Italiano, IRCCS, Center for Cardiac Arrhythmias of Genetic Origin and Laboratory
4   of Cardiovascular Genetics, 22 Via Pier Lombardo, Milan, Italy
5   [21] Istituto Auxologico Italiano, IRCCS, Cardiomyopathies Unit, Department of Cardiovascular, Neural
6   and Metabolic Sciences, San Luca Hospital, Milan, Italy
7   [22] Department of Medicine and Surgery, University of Milano-Bicocca, Milan, Italy
8   [23] BIOSS, Center for Biological Signaling Studies, University of Freiburg, 79104 Freiburg, Germany
9   [24] Department of Surgery, Yale University, New Haven, CT, USA
10
11   † These authors contributed equally to this work.
12   * Co-corresponding authors
13

14

15

1 **ABSTRACT**

2

3 **Background:** Complex molecular programs in specific cell lineages govern human heart

4 development. Hypoplastic left heart syndrome (HLHS) is the most common and severe

5 manifestation within the spectrum of left ventricular outflow tract obstruction defects occurring

6 in association with ventricular hypoplasia. The pathogenesis of HLHS is unknown, but

7 hemodynamic disturbances are assumed to play a prominent role.

8 **Methods:** To identify perturbations in gene programs controlling ventricular muscle lineage

9 development in HLHS, we performed: i) whole-exome sequencing of 87 HLHS parent-

10 offspring trios, ii) nuclear transcriptomics of cardiomyocytes from ventricles of 4 patients with

11 HLHS and 15 controls at different stages of heart development, iii) single cell RNA

12 sequencing and iv) 3D modeling in iPSCs from 3 patients with HLHS and 3 controls.

13 **Results:** Gene set enrichment and protein network analyses of damaging *de-novo* mutations

14 and dysregulated genes from ventricles of patients with HLHS suggested alterations in

15 specific gene programs and cellular processes critical during fetal ventricular cardiogenesis,

16 including cell-cycle and cardiomyocyte maturation. Single-cell and 3D modeling with iPSCs

17 demonstrated intrinsic defects in the cell-cycle/UPR/autophagy hub resulting in disrupted

18 differentiation of early cardiac progenitor lineages leading to defective cardiomyocyte-

19 subtype differentiation/maturation in HLHS. Additionally, premature cell-cycle exit of

20 ventricular cardiomyocytes from HLHS patients prevented normal tissue responses to

21 developmental signals for growth leading to multinucleation/polyploidy, accumulation of DNA

22 damage, and exacerbated apoptosis, all potential drivers of left ventricular hypoplasia in

23 absence of hemodynamic cues.

24 **Conclusions:** Our results highlight that despite genetic heterogeneity in HLHS, many

25 mutations converge on sequential cellular processes primarily driving cardiac myogenesis,

26 suggesting novel therapeutic approaches.

27

INTRODUCTION

HLHS is a severe form of congenital heart disease (CHD) characterized by underdevelopment of left-sided cardiac structures, including left ventricular (LV) hypoplasia, hypoplastic ascending aorta, intact interventricular septum, aortic and/or mitral valve atresia/stenosis in the setting of concordant ventriculoarterial connections[1-3]. Although a genetic etiology is supported by an increased recurrence risk and familial clustering, the largely sporadic occurrence suggests a complex genetic model[4,5].

Historically, ventricular and aortic hypoplasia in HLHS has been attributed to reduced growth arising as consequence of restricted blood flow due to maldeveloped mitral and/or aortic valve[6,7]. Recently, an anatomic study of HLHS hearts indicated that ventricular and valvular morphology are poorly correlated and three phenotypic LV variants ("slit-like", "thickened", and "miniature") are present, extending earlier suggestions that a pathogenic mechanism based upon reduced blood flow alone may be insufficient[8,9]. In the *Ohia* mouse model specific mutations drive LV hypoplasia by perturbing cardiomyocyte (CM) proliferation/differentiation[10]. The large majority of *Ohia* mutants display HLHS, although some mutants can have double-outlet right ventricle that do not uniformly resemble human HLHS pathology. Interestingly,, transcriptional alterations found in the LV of the *Ohia* mice with HLHS are present, though less severe, in the right ventricle (RV). This finding suggests that intrinsic defects in myogenic programs of both ventricles may manifest differently, depending on combinations of the cardiac progenitor (CP) population affected and physiological milieu.

During cardiogenesis, two main CP lineages provide CMs to the developing heart with distinct temporal and spatial contributions[11]. The first heart field (FHF) CPs are fated to differentiate early forming the primitive heart tube, the LV, and portion of the atria, while the second heart field (SHF) cells show delayed differentiation into CMs and represent initially a reservoir of multipotent CPs[12,13]. Later, SHF CPs give rise to the RV, the proximal outflow tract (OFT), and part of the atria[14].

4

1   Elegant work using CMs derived from human iPSCs has recently begun to elucidate

2   molecular mechanisms of CHD in patient-specific *in-vitro* models of cardiogenesis[15,16].

3   Studies in iPSC-CMs from HLHS patients carrying variants in the NOTCH signaling pathway

4   demonstrated impaired differentiation[17-19]; other studies implicated transcriptional repression

5   of *NKX2-5*, *HAND1*, and *NOTCH1* or activation of atrial gene programs[20,21]. Still lacking is a

6   unifying picture of how the profound genetic heterogeneity of HLHS converges in common

7   perturbations of sequential cellular processes driving heart morphogenesis, how these

8   processes are altered, and how such alterations contribute to the disease.

9   Here, we combined whole-exome sequencing (WES) of parent-offspring trios,

10   transcriptome profiling of CMs from ventricular biopsies, iPSC-derived CP/CM models of

11   2D/3D cardiogenesis, and single-cell gene expression analysis to decode the cellular and

12   molecular principles of HLHS phenotypes. Our results show that initial aberrations in the cell-

13   cycle/UPR/autophagy hub lead to disrupted CP lineage commitment. Consequently, impaired

14   maturation of ventricular CMs (vCMs) limits their ability to respond to growth cues resulting in

15   premature cell-cycle exit and increased apoptosis under biomechanical stress in 3D heart

16   structures. Together, these studies provide evidence that HLHS pathogenesis is not

17   exclusively of hemodynamic origin, and reveal novel potential nodes for rational design of

18   therapeutic interventions.

1 **METHODS**

2

3 **Data availability**

4 All data needed to evaluate the conclusions of this study are present in the article or the Data

5 Supplement. The raw omics data have been deposited at public available databases (bulk

6 and scRNAseq, #GSE135411; nRNAseq, #PRJNA353755; proteomics, #PXD014812).

7

8 **Patients and controls**

9 All HLHS patients harbored hypoplastic LV and ascending aorta, mitral and/or aortic valve

10 atresia/stenosis, and intact interventricular septum. Two additional patients with LV

11 hypoplasia and a ventricular septal defect not meeting strict HLHS criteria were included in

12 the WES analysis but not selected for further analyses.

13 Blood for WES was collected from 87 probands with sporadic HLHS and their respective

14 parents (clinical information are summarized in Table I Supplement). Human heart ventricular

15 samples from control and HLHS patients were obtained from aborted fetuses or during the

16 Norwood Stage-I palliation. All donors or their legal representatives provided informed

17 consent. The study was performed according to the Declaration of Helsinki and approved by

18 the local ethics committees at the respective institutions (KaBi-DHM: 5943/13, 247/16S; IHG:

19 5360/13; HSM:15-00696).

20

21 **Statistics**

22 Statistical analyses were performed using R and Graphpad Prism. Data were analyzed with

23 ANOVA , Kruskal-Wallis, Mann–Whitney, Chi-square, Fisher's, and Student's t test, as

24 appropriate. P values and p adjusted of less than 0.05 were considered statistically

25 significant.

26

1   **RESULTS**

2

3   **Damaging *de-novo* mutations in HLHS patients are linked to cardiac development,**

4   **chromatin organization, and cell-cycle phases**

5   WES from 87 patients with sporadic HLHS and their parents recovered 94 non-synonymous

6   (NS) *de-novo* mutations (DNMs), of which 12 were loss-of-function (LOF) and 76 predicted

7   damaging missense (D-Mis) variants (Table I Supplement). One to five NS-DNMs were

8   found in 56 cases (Figure IA and IB Supplement). Among the 51 cases with D-DNMs, 34

9   carried mutations in genes or HGNC gene families that harbored multiple hits (Figure 1A). D-

10   DNMs in *MYRF*, *MACF1*, and *LRP6* were found twice, with 2 individuals carrying variants in

11   2 of the 3 genes (Figure 1A). *MYRF* was recently associated with CHD[22] and HLHS[23]. *LRP6*

12   and *MACF1* are linked to WNT signaling[24,25]. Gene-families with multihits were likewise

13   related to pivotal signaling pathways implicated in cardiac development (Hedgehog, FGF,

14   and NOTCH) or to the histone modification H3K4me-H3K27me pathway that has been

15   associated with CHD[26,27].

16   Analyzing single-cell transcriptomics from human embryonic (4.5–25 weeks post-

17   conception) cardiac cells[28,29], we found 96% of the 84 D-DNM genes expressed in different

18   cell types, significantly more than random gene sets (76.7%±8.8%, *p*-value <10e-15).

19   Interestingly, high expression was observed in at least one stage of chamber or OFT

20   development (Figure 1B and Figure I Supplement), suggesting an intrinsic CM lineage

21   dysfunction as a possible determinant of HLHS. GSEA of D-DNM genes revealed a

22   significant enrichment in gene categories related to cardiac and embryonic

23   development/growth, cell fate commitment/differentiation as well as cell-cycle and G1/S

24   phase transition (E2F pathway) (Figure 1C and Table I Supplement). Network analysis

25   identified 12 interconnected protein-protein interaction modules (0.63 modularity; 11.84

26   scaled-modularity) significantly different from random networks (0.36±0.023 modularity

27   (n=100, mean±SD); *p*-value <10e-05), comprising 32 of the 84 D-DNM genes (Figure 1D).

28   Genes in these modules act in biological processes critical for CP specification and CM

1   maturation, including cell-cycle and apoptosis, response to endoplasmic reticulum (ER)

2   stress, signaling by Smoothened, WNT, FGF, and NOTCH, transcriptional regulation, and

3   histone methylation.

4   Additionally, we interrogated independent 459 HLHS parents-offspring trios within the

5   CHD cohort of the Pediatric Cardiac Genomics Consortium (PCGC)[27] for *de-novo* variants.

6   The occurrence of NS-DNMs and the distribution of variant classes were comparable, with 3

7   genes related to known syndromic forms of CHD (*CHD7*, *KMT2D*, and *MYRF*) being

8   common D-DNM multihits (Figure IIA through IIC Supplement). GSEA and network

9   interactome analyses of the combined cohort yielded similar results to our cohort alone

10   (Figure IID and IIE Supplement). Importantly, compared to 1789 control trios comprising

11   parents and unaffected siblings of autism probands[30], most GSEA retrieved pathways

12   showed significant burden enrichment in D-DNMs among cases (Figure IID Supplement).

13   Randomization of DNMs between HLHS and controls confirmed the non-stochastic nature of

14   our results (Table I Supplement).

15

16   **Dysregulated genes in infant HLHS CMs belong to dynamic transcriptional networks**

17   **during cardiogenesis**

18   To verify dynamic expression of HLHS D-DNM genes during CM development and identify

19   temporal/spatial processes of cardiogenesis critical to HLHS pathogenesis, we performed

20   nuclear RNA sequencing (RNAseq) of RV CMs from healthy hearts at 3 developmental

21   stages – *fetal* (16-23 weeks post-conception), *infancy* (10 weeks to 10 months), and

22   *adulthood* (21-50 years) – and from infant HLHS subjects (5-11 days of age) (Figure 2A and

23   Table II Supplement). The choice of RV tissue was based on the fact that LV is inaccessible

24   from living HLHS subjects and that both ventricles may share altered transcriptional

25   signatures, as found in *Ohia* mutants.

26   We first compared RV tissues from the 4 normal and 4 HLHS infants, who presented

27   "thickened" morphological features of the hypoplastic LV[8,9] (Figure 2B). An equal proportion

28   of CM nuclei was found in both groups (Figure IIA Supplement). HLHS CMs showed a

8

1   significant increase in the number of tetraploid nuclei at the expense of diploid nuclei (Figure

2   2C). Since polyploidization accompanies terminal CM differentiation and permanent cell-

3   cycle withdrawal[31], this suggests premature cell-cycle arrest in HLHS. RNAseq analysis

4   revealed 2,286 differentially expressed genes (DEGs) in HLHS compared to controls (Figure

5   2D and Table II Supplement). Comparative principal component analysis (PCA) clearly

6   separated HLHS and controls (Figure 2E). Enrichment Map of the Gene Ontology (GO)

7   categories recovered from DEGs demonstrated high interconnection of functionally related

8   gene sets associated with cell-cycle/mitotic-checkpoints, response to stimuli/stress, organ

9   development, cell differentiation/apoptosis, cytoskeleton/microtubule/nucleus, and regulation

10   of metabolism (Figure 2F and Table II Supplement). Importantly, most pathways overlapped

11   with the modules recovered from the HLHS D-DNM genes. In HLHS, GSEA revealed

12   reduced expression of genes important for cardiac ventricle morphogenesis and increased

13   expression of genes controlling DNA repair (Figure 2G). Moreover, negative regulators of cell

14   division were upregulated, while genes associated with muscle cell proliferation were down,

15   supporting the notion of premature cell-cycle exit.

16   To assess whether DEGs and D-DNM genes in HLHS are dynamically regulated

17   during development, we next established a global expression atlas of *fetal*, *infant* and *adult*

18   healthy RV genes. Hierarchical clustering demonstrated distinct expression profiles among

19   developmental stages (Figure IIIB Supplement). Investigation of DEGs identified 10

20   transcriptome clusters dynamically changing during cardiac development (Figure IIIC

21   Supplement). DEGs in HLHS infants resembled the *fetal* rather than the *infant* stage (Figure

22   2H). Remarkably, 60% of HLHS downregulated DEGs belonged to dynamic transcriptome

23   clusters, being 56% distributed in gene clusters 1, 2, 3, and 6. These contained genes

24   upregulated from the embryonic to newborn phases and mainly involved in cellular transport

25   and metabolic processes (Figure 2I, Figure IIIC and Table II Supplement). Furthermore, 21%

26   of the upregulated transcripts fitted to clusters 5 and 7, representing genes regulating

27   morphogenesis and cell-cycle and whose expression levels decreased in infant stage (Figure

1   2I, Figure IIIC and Table II Supplement). Concordantly, 22 of the 84 D-DNM genes in our

2   HLHS cohort were found in most clusters.

3   Together, these findings indicate that HLHS may result from alterations in specific

4   gene programs critical during fetal ventricular cardiogenesis and suggest a role of cell-cycle

5   and CM maturation as potential disease drivers.

6

7   **Specific gene networks are dynamically altered during differentiation of HLHS iPSCs**

8   **towards CPs and CMs**

9   To better dissect to which extent transcriptional alterations of native HLHS CMs underlie

10   disease pathogenesis rather than physiological differences at the time of RV sampling, we

11   generated iPSCs from 3 HLHS patients and 3 healthy subjects using Sendai-mediated

12   reprogramming (Figures IV and V Supplement) and mechanistically analyzed developmental

13   processes during early *in-vitro* cardiogenesis. Selection of HLHS patients was based on

14   echocardiographic LV morphology ("thickened" phenotype) and presence of D-DNMs in

15   genes affected twice or belonging to multihit gene families (Figure VI Supplement).

16   Control and HLHS iPSC lines were directed to early CPs[32] and CMs[33] using stepwise

17   differentiation protocols (Figure 3A). We performed RNAseq at various time points and

18   explored functional characteristics of HLHS DEGs by GSEA (Figure 3B and Table III

19   Supplement). Dynamic alterations in several gene categories were common in both CP and

20   CM differentiation protocols, including heart/aorta development, cell-cycle, and chromatin

21   modification. Interestingly, unique aberrations in autophagy terms were present when

22   directing HLHS iPSCs towards early CPs, while apoptosis-associated pathways appeared

23   solely affected in later CPs (D6) and CMs (D8 and D14) (Figure 3B and Table III

24   Supplement).

25   In CPs at D2 and D3, detailed analysis of DEGs involved in cardiac development

26   revealed that genes expressed in committed myocytic precursors and important for heart

27   tube formation (e.g. *ID2*, *TPM2*, *XIRP1*, *SRF, ETV1*) were downregulated in HLHS, while

28   genes involved in anterior/posterior patterning (*HOXB9*) and in vessel/valve development

10

1   (*VEGFB*, *TGFB2*, *GATA5*) were upregulated (Figure 3C). Transcripts typical of early CPs

2   were decreased at D2, but augmented at D3, suggesting incomplete/delayed CP lineage

3   specification. Concordantly, at D8 and D14, HLHS CMs showed upregulation of genes

4   distinctive of myocytic progenitors/early immature CMs and altered expression of transcripts

5   important for OFT and atrioventricular-canal (AVC) (*MEIS1*, *ISL1*, *TGFB2*, and *JUN*) as well

6   as heart chamber development (*NR2F1*, *WNT2*, *ETV2*, *RXRA*) (Figure 3C and Table III

7   Supplement), supporting dysregulated lineage-specific CM differentiation.

8   In CPs at D3, 74 of the 890 DEGs related to cell-cycle GO categories (Figure VIIA

9   and Table III Supplement). Thirty-four of them generated a functional interactome network

10   encompassing cell-cycle interphase pathways as the top enriched, with most leading genes

11   being downregulated (Figure 3D and Table III Supplement). In CMs at D14, cell-cycle DEGs

12   (42/754) generated 18 functional interaction nodes; top enriched terms within the interactome

13   and regulation of the leading genes pointed to alteration in M phase, with active separation of

14   chromatids (*STAG2*, *XPO1*) but defective progression through mitosis (*ANAPC5*) and

15   cytokinesis (*AURKC*) (Figure 3D and Table III Supplement). Cell-cycle defects in HLHS CMs

16   were also confirmed by proteomic analysis (Expanded Results, Figure VIII, and Table III

17   Supplement).

18   Together, the specific transcriptional alterations detected during early CP

19   specification and CM differentiation of HLHS iPSCs suggest the primary onset of the disease

20   occurs at the initial stages of cardiogenesis when CM lineage decisions arise within CP

21   populations.

22

23   **Defects in UPR-induced autophagy lead to delayed and disrupted CP lineage**

24   **specification**

25   To investigate the role of cell-cycle disturbances in HLHS pathogenesis, we analyzed cell-

26   cycle patterns during early CP formation and compared them with the emergence of CP

27   lineages marked by ISL1, NKX2-5, and TBX5. While control lines demonstrated G1

28   lengthening starting between D1 and D2, patient lines prolonged G1 phase with a 24h delay

1   (Figure 4A). Concurrently, at D1, activation of *ISL1* and *NKX2-5* transcripts was dramatically

2   reduced in HLHS (Figure VIIB Supplement) and correlated with significant lower proportions

3   of cells expressing ISL1 and NKX2-5 proteins at D2 (Figure 4B), supportive of a retarded CP

4   specification. Interestingly, four patterns of ISL1 and NKX2-5 expression were detected at

5   D3: **i**) ISL1^{low}/NKX2-5^{low}, representing "early committed CPs"; **ii**) ISL1^{high}/NKX2-5^{high}, denoting

6   "fully committed early CPs"; **iii**) ISL1^{high}/NKX2-5^{low}, typical of SHF progenitors; and **iv**)

7   ISL1^{low}/NKX2-5^{high}, distinctive of FHF cells (Figure 4C). TBX5, a specific FHF marker, was

8   mainly found in ISL1^{low}/NKX2-5^{high} cells (Figure 4C), confirming FHF identity. The relative

9   distribution of CP subgroups was altered in HLHS settings (Figure 4D). Importantly, all HLHS

10 lines failed to upregulate *TBX5* during CP specification (Figure VIIB Supplement) and only

11 few of the ISL1^{low}/NKX2-5^{high} FHF cells expressed TBX5 (Figure 4E), indicating common

12 defective transcriptional programs within the FHF lineage. To assess the contribution of

13 apoptosis/proliferation to the observed CP phenotypes, we analyzed caspase-3 activation

14 and EdU incorporation. Apoptosis was barely detectable in both HLHS and controls (Figure

15 VIIC Supplement), arguing against any cell selection of HLHS CPs. Consistent with the

16 alteration in cell-cycle patterns, global changes in cell proliferation rates between control and

17 HLHS were only significantly different at D2 (Figure VIID Supplement). However, when

18 analyzed separately at D3, ISL1^{low}/NKX2-5^{high} FHF progenitors demonstrated higher

19 proliferation in all HLHS lines (Figure 4F), consistent with the reported role of TBX5 as

20 negative regulator of cell proliferation during early cardiac development[34]. Collectively, these

21 data indicate common defects in CP lineage commitment and imbalance of both progenitor

22 fields during initial steps of HLHS cardiogenesis.

23   Autophagy and cell-cycle are coordinated and reciprocally regulated[35]. Since

24 autophagy was altered in HLHS CPs from D1 on (Figure 3B), we measured autophagic flux

25 in cells at D3 by analyzing the levels of LC3II, a marker of autophagosomes, and p62, a

26 substrate for autophagic degradation. Under basal conditions, LC3II and p62 proteins were

27 normal in all HLHS lines (Figure 4G and Figure VIIE Supplement). However, after activation

28 of autophagy (starvation or brefeldin-A), defective autophagosome formation and p62

12

1   degradation were evident in all HLHS lines (Figure 4G). This was also confirmed by Cyto-ID

2   staining of autophagic vacuoles (Figure VIIF Supplement). Brefeldin-A triggers autophagy *via*

3   ER stress and activation of the unfolded protein response (UPR)[36], a pathway also

4   challenged by starvation. UPR plays an important role in cell fate acquisition of embryonic

5   stem cells and progenitors[37-39]. Given the recovery of HLHS D-DNMs in ER-stress/UPR

6   genes (Figure 1D and Table I Supplement), we asked whether the defective autophagy in

7   HLHS CPs is caused by impaired UPR. Upon ER stress, UPR is transduced by de-

8   repression of three ER membrane proteins: IRE1α, PERK, and ATF6 that work alone or in

9   concert to restore normal cellular function[40]. Interestingly, neither an increased splicing of

10   *XBP1* mRNA, which occurs downstream of IRE1α stimulation, nor activation of *ATF6* were

11   altered in HLHS CPs at D3 upon brefeldin-A treatment (Figure VIIG Supplement). Instead,

12   we measured a specific common defect of all HLHS lines in activating the PERK pathway, as

13   indicated by decreased PERK-mediated phosphorylation of eIF2α (Figure VIIH Supplement)

14   and reduced increase of *ATF4* and its downstream targets including *CHOP* (Figure 4H and

15   Figure VIIG Supplement). A six-hour treatment of HLHS cells with the selective PERK

16   activator CCT020312 normalized *ATF4* and *CHOP* levels and rescued the defective

17   activation of autophagy (Figures 4I and 4J). Importantly, early application of CCT020312 at

18   D1.5 of CP differentiation was sufficient to revert the HLHS phenotype, as indicated by

19   normalization of the number of cells in G1 at D2 and the level of *TBX5* at D3 (Figure 4K).

20   Conversely, HLHS-like disturbances in G1-phase lengthening and *TBX5* upregulation could

21   be induced in control cells by inhibiting autophagy at D1.5 using chloroquine, with no

22   influence on *ISL1* expression (Figure VIII Supplement).

23   Taken together, these results suggest that defects in UPR/autophagy activation in the

24   early phase of CP specification contribute to delayed and disrupted CP lineage commitment

25   in HLHS.

26

27   **Single-cell RNAseq defines impaired CM lineage segregation and maturation in HLHS**

13

1   To investigate the consequences of altered CP specification on CM-subtype formation, we

2   performed single-cell RNAseq of early CMs at D14. Transcriptomes of 6,431 control and

3   4,439 HLHS cells were recovered. Unsupervised clustering analysis identified 10 distinct

4   sub-populations (clusters 0-9) (Figure 5A and Table III Supplement). We assigned identities

5   to each population by cross-referencing the most highly and uniquely expressed genes in

6   each cluster with known cardiac subtype markers from human and mouse single-cell studies

7   (Figure 5B and Expanded Results Supplement)[28,29,41-43]. We captured transcriptome

8   characteristics of primary (OFT and AVC) and chamber myocardium, early and late CPs,

9   maturing CMs, and proliferating CMs in G1/S and G2/M phases (Figure 5A through 5C and

10   Figure IXA Supplement). Remarkably, HLHS cells contributed almost exclusively to CP

11   clusters (cluster 7: CTR=40, HLHS=450; cluster 9: CTR=35, HLHS=117) and were strongly

12   under-represented in the cluster containing terminally differentiated CMs (cluster 8:

13   CTR=318, HLHS=37), together suggestive of an intrinsic differentiation delay. Moreover, we

14   noticed a significant reduced proportion of HLHS cells in the proliferating cell clusters (cluster

15   4: CTR=922, HLHS=284; cluster 6: CTR=675, HLHS=103), corroborating a premature cell-

16   cycle exit in HLHS CMs. Interestingly, co-expression of LV enriched genes was observed

17   mainly in CMs of cluster 0 that was scarce in HLHS cells (cluster 0: CTR=1446, HLHS=497).

18   This correlated with an overall downregulation of LV transcripts in HLHS (e.g. *TBX5*, *HAND1*,

19   *SLIT2*, *GJA1*) (Figure IXB Supplement), hinting to a potentially reduced LV commitment.

20   Differential expression analysis within each cluster revealed increased levels of pro-apoptotic

21   genes (*TNFRSF12A*, *FAM162A*) and reduced expression of anti-apoptotic regulators (e.g.

22   *MTRNR2L1*) in HLHS CMs (Figure 5D and Figure IXC Supplement), confirming bulk RNAseq

23   results. Moreover, HLHS CMs presented an overall upregulation of genes involved in

24   glucose catabolism, downregulation of mitochondrial transcripts, and lower expression of

25   sarcomeric genes; exceptions were *MYL7* and *TNNI1*, isoforms highly expressed in

26   immature CMs (Figure 5D and Figure IXC and IXD Supplement), collectively suggesting

27   reduced cellular differentiation/maturation. To further verify this, we used recently published

28   single-cell profiles of healthy iPSC-CMs at different stages of differentiation[44]. We ordered

1 CMs captured at D5 and D14 together with our cells in pseudotime. The resulting

2 differentiation trajectory began with CM at D5 and bifurcated into two lineages where CMs at

3 D14 were allocated (Figure 5E). Importantly, a large proportion of HLHS CMs, although at

4 D14, clustered with D5 CMs and expressed high level of *KRT19*, a gene specific of early

5 immature CMs (Figure 5E).

6 Together, these results indicate that both early CM-subtype lineage specification and

7 CM differentiation/maturation are disrupted in HLHS. Moreover, they confirm, at a single-cell

8 transcriptional level, a premature cell-cycle withdrawal in diseased CMs.

9

10 **3D heart patches unravel dysregulated nodes for CM contractility, maturation, and**

11 **survival in HLHS**

12 We further analyzed HLHS phenotypes in a multicellular 3D context by repopulating

13 decellularized scaffolds from non-human primate LV heart slices with early D14 iPSC-CMs.

14 Standardized cell seeding was achieved using bioprinting and constructs underwent

15 electromechanical conditioning (1Hz pacing, 1mN diastolic preload) in customized

16 biomimetic chambers[45] for 24 days (Figure 6A). Contractile force of HLHS patches was

17 significantly reduced compared to controls and did not increase, but rather decreased,

18 overtime (Figure 6B and 6C). Moreover, while progressive electromechanical maturation was

19 evident in controls, HLHS tissues failed to respond to high stimulation frequencies and to

20 develop a positive force-frequency relationship (Figure 6D through 6F). Concurrently, Ca^{2+}

21 imaging of single CMs within the patches demonstrated a gradual decline in the number of

22 electrically responsive HLHS cells (Figure 6G through 6I) and intrinsic Ca^{2+} handling defects,

23 with failed increase of systolic and abnormal elevation of diastolic Ca^{2+} at high stimulation

24 rates (Figure 6J and 6K). Expression profile of HLHS CMs isolated from 3D patches at D12

25 confirmed inherent molecular changes of pivotal genes involved in electromechanical

26 coupling and Ca^{2+} homeostasis (Figure 6L). Moreover, live evaluation of cell viability

27 revealed a progressive increase of dead cells in HLHS tissues (Figure XA Supplement),

28 suggesting apoptosis as additional mechanism underlying the functional deterioration.

15

1   Immunohistochemistry demonstrated a gradual increase of apoptotic CMs

2   (clCasp3[+]/TUNEL[+]) in diseased patches (Figure 7A). Intriguingly, not all TUNEL[+] CMs

3   expressed activated caspase-3, while the opposite was true; moreover, the percentage of

4   clCasp3[-]/TUNEL^{+} cells was also significantly elevated in HLHS (Figure 7A), indicating

5   apoptosis-independent DNA damage. To better assess this, we performed co-

6   immunofluorescence analysis of activated caspase-3 and activated p53 (phP53), a tumor

7   suppressor that induces either cell-cycle arrest to facilitate DNA repair or apoptosis[46]. We

8   detected clCasp3[+]/phP53[+] and clCasp3[-]/phP53[+] CMs, with a significant increase of both in

9   HLHS tissues (Figure 7B). Notably, the percentage of clCasp3[-]/phP53^{+} cells matched well

10   with the proportion of clCasp3[-]/TUNEL^{+} cells, suggesting that DNA damage might be the first

11   event leading to apoptosis of HLHS CMs.

12   An interesting finding emerging from histological analyses was abnormal

13   multinucleation of CMs in HLHS patches, already evident at D12 (Figure 7C). Polyploidy and

14   binucleation are characteristic features of mammalian CMs that develop shortly after birth

15   when most differentiated CMs exit cell-cycle[31]. In humans, polyploidy is often increased in

16   pathological conditions; however, binucleation occurs in only 25% CMs, with no evidence of

17   tri- or tetranucleation[47]. In control patches, most CMs carried 1 (~70%) or 2 (~25%) nuclei,

18   and only few cells presented 3 or more; conversely, in HLHS tissues, ~50% of CMs were

19   tri/tetranucleated (Figures 7C and 7D), indicating an intrinsic failure to complete cytokinesis

20   and premature cell-cycle withdrawal. Markers of cell-cycle activity (Ki67) and mitosis

21   (phospho-histone H3, PH3) demonstrated an overall increase in the number of active CMs in

22   HLHS patches, with the proportion of cells in mitosis being similar (Figure 7E). However,

23   detailed analysis of Ki67 and PH3 expression revealed that, in mononucleated CMs, most

24   nuclei were in M phase (Ki67^{+}/PH3^{+}) and their percentage was higher in HLHS (Figure 7F).

25   Importantly, greater the degree of multinucleation in HLHS, higher was the proportion of

26   Ki67^{+}/PH3^{-} *vs* Ki67^{+}/PH3^{+} nuclei (Figure 7F), suggesting that polyploidization was also

27   occurring in multinucleated diseased CMs. To assess whether and how the abortive cell-

28   cycle mode of HLHS CMs related to apoptosis, we evaluated the distribution of TUNEL[+]

16

1   nuclei and clCasp3$^+$/TUNEL$^+$ cells (Figure 7G). We found a striking correlation between the

2   number of TUNEL$^+$ nuclei and the level of multinucleation, being most damaged nuclei in the

3   tri-/tetranucleated CMs. The latter showed also the highest percentage of activated caspase-

4   3 (Figure 7G), together indicating chromosomal instability acquired during aberrant cell-cycle

5   as possible apoptotic trigger in HLHS CMs.

6   We hypothesized that the observed HLHS CM phenotype might be a specific reaction

7   to strong cues for cell division/growth and maturation, which are provided by the

8   electromechanical preconditioning in the 3D-tissue environment. Since our transcriptome

9   profiling of early HLHS CMs developed in 2D-monolayer pointed to defects in

10   differentiation/maturation, we performed co-immunofluorescence analysis for MLC2a

11   (expressed in all immature CMs and becoming atrial-specific after terminal chamber

12   differentiation) and MLC2v (expressed in maturing vCMs). In HLHS patches, we measured a

13   striking increase of MLC2a$^+$ cells with reduction of MLC2v$^+$ CMs at D12 and D24 (Figure 7H);

14   moreover, sarcomere organization was impaired (Figure XB Supplement), indicative of

15   reduced maturation. Similar results were obtained in HLHS CMs (D30 and D60) in 2D-

16   monolayers (Figure XC through XE Supplement). Expression analysis of terminally

17   differentiated atrial, ventricular, and CM maturation markers confirmed that the abnormal

18   distribution of HLHS MLC2a$^+$/MLC2v$^+$ cells was a result of defective ventricular

19   differentiation/maturation rather than an atrial lineage switch (Figure XF Supplement). This

20   was corroborated by measuring intracellular Ca^{2+} cycling of 2D CMs (Figure XIA through XIC

21   Supplement). Importantly, no aberrant multinucleation or apoptosis were visible in 2D (Figure

22   XID through XIF Supplement).

23   Together, these results indicate that impaired maturation and inability to respond to

24   cues for developmental growth by normal progression through cell-cycle leads to increased

25   apoptosis of vCMs contributing to HLHS pathogenesis.

1 **DISCUSSION**

2

3 Our work provides a multidisciplinary framework for studying human heart development and

4 its disruption in CHD. WES of HLHS parent-offspring trios and transcriptomics of patient RV

5 CMs identified consistent perturbations in gene expression programs and associated

6 features of abnormal cardiac development. Human iPSC lines derived from HLHS patients

7 facilitated dynamic evaluation of transcriptional and cellular phenotypes during progression of

8 cardiogenesis in single cells and 3D functional modeling of ventricular chamber

9 development. Together, our data indicate that initial perturbations of the cell-

10 cycle/UPR/autophagy hub result in disrupted differentiation of early CP lineages and

11 disproportionate allocation of vCM-subtypes in HLHS. Moreover, impaired maturation and

12 premature cell-cycle exit of vCM reduce their ability to respond to cues for tissue growth

13 resulting in increased apoptosis and ventricular hypoplasia (Figure 7I).

14

15 **Identification of dysregulated transcriptional nodes in HLHS**

16 Pathway analysis of D-DNMs in HLHS cases showed significant enrichment in heart

17 development and its related signaling pathways. Comprehensive investigation of single-cell

18 expression profile and dynamically regulated gene programs in CMs indicated an occurrence

19 of D-DNMs in gene modules typical of the embryonic stage encompassing cell-cycle.

20 Transcriptomes of infant HLHS vCMs closely resembled a fetal stage, demonstrating that

21 embryonic gene programs persist in HLHS CMs after birth. We identified dysregulated

22 transcriptional nodes common to both CP and CM states or unique of one state. Moreover,

23 single-cell RNAseq of HLHS CMs recognized distinct regulatory defects in specific cellular

24 subsets indicating that both early CM-subtype lineage specification, maturation and cell-cycle

25 are disrupted in the disease.

26 Previous studies in HLHS iPSCs showed reduced cardiac differentiation and

27 structural CM maturation in presence of dysfunctional NOTCH signaling[17-19] and suggested

28 defective commitment to the ventricular lineage[21], corroborating our results. Moreover,

18

1   abnormalities in endocardial cells were shown to influence CM proliferation/maturation in

2   HLHS[48].

3   Evidence of cell-cycle arrest and impaired maturation has been reported in vCMs of

4   the hypoplastic LV of HLHS fetuses[49] and *Ohia* mutants[10]. Loss of replication potential during

5   fetal growth likely impacts cardiac chamber development and function. Indeed, our 3D

6   functional studies revealed, both on the tissue and single CM level, abnormalities of

7   excitation-contraction coupling reminiscent of failing human myocardium. Beside the valvular

8   perturbations, chamber-specific differences in proliferation rates at early stages of

9   development may explain why loss of CM proliferation in HLHS affects LV more than RV. By

10   analyzing cell-cycle gene signature of single CMs from RV and LV regions of human

11   embryonic hearts from 5 to 25 weeks of gestation[29], we found LV CMs proliferate more than

12   their RV counterpart at 5 weeks (58% LV *vs* 48% RV), but these differences extinguish later

13   in development (45% and 55% LV *vs* 43% and 53% RV at 6 and 7 weeks, respectively).

14   Concordantly, similar analysis using our single-cell RNAseq data of D14 control iPSC-CMs

15   with LV and RV transcriptome revealed a ~3-fold increased proliferation of LV compared to

16   RV cells (34.5% LV *vs* 11.8% RV, p<0.05).

17

18   **Linking clinical phenotype to mechanism**

19   HLHS is a spectrum of disease that includes LV and aortic hypoplasia with aortic and mitral

20   valve malformations ranging from stenosis to complete atresia. Historically, the "flow-volume

21   hypoplasia" hypothesis has been supported by experiments in multiple model systems.

22   However, recent observations in patients[8,9] argue that hemodynamic conditions alone are

23   insufficient to explain variable LV morphology. We focused on the "thickened" LV morphology

24   with a clearly visible LV lumen[8,9] and were able to identify a common mechanism (Figure 7I)

25   for the initial arrested LV development in this specific anatomic subtype. Intrauterine, fetal

26   valvuloplasty in HLHS patients is being studied as treatment option to enable LV growth.

27   However, the existence of intrinsic CM defects such as loss of replication and increased

28   apoptosis in distinct subsets of HLHS patients suggest a way to potentially improve the

19

1 unpredictable results of this aortic valvuloplasty approach[50]. Furthermore, knowledge of

2 these specific defects allows development of rational strategies, either by stratification or

3 adjunctive therapies, potentially permitting biventricular repair in those with less serious

4 forms of LV hypoplasia.

5

6 **Limitation of the study**

7 The small number of our HLHS parent-off-spring trios limited identification of new disease

8 candidate genes. Regardless, the combination of WES data from our and the PCGC HLHS

9 cohorts identified disturbed genetic pathways with significant burden enrichment in D-DNMs,

10 which we functionally validated.

11 The inability to obtain LV samples from HLHS patients, differences in RV *vs* LV physiology,

12 age, medications, and the intrinsic variability among different iPSC lines are potential

13 confounders. However, the recovery of consistent molecular and cellular alterations in native

14 RV CMs and *in-vitro* iPSC models reinforces their causal relation to HLHS pathogenesis.

15

16 Taken together, our results suggest that a shared mechanism for subsets of HLHS.

17 Moreover, they highlight that reduced LV growth in HLHS is likely not the sole consequence

18 of disrupted valve formation and impaired blood flow; instead, intrinsic defects of vCM

19 lineage development are primary contributors to the disease pathogenesis. More broadly, our

20 work illustrates that, despite the extensive genetic heterogeneity underlying CHD, studying

21 cardiac developmental processes in CHD patients using converging multidimensional

22 technologies can provide deep mechanistic insight into these complex diseases to suggest

23 novel therapeutic approaches.

1   ACKNOWLEDGMENTS

2   We thank the HLHS family members from the US and Europe and the healthy volunteers for

3   participation in our study. We would like to thank A.M., M.K., and P.J.G. lab members for

4   technical assistance, helpful suggestions, and discussions. We would like to acknowledge

5   Birgit Campbell and Christina Scherb for their technical assistance in cell culture, Gabi

6   Lederer (Cytogenetic Department, TUM) for karyotyping, members of the KaBi DHM Biobank

7   for patient sample collection, Alma Kuechler (Institute of Human Genetics, University

8   Hospital Essen) for providing one HLHS trio, and Rabea Hinkel (Deutsches Primatenzentrum

9   Göttingen) for providing NHP heart samples.

10   SOURCES OF FUNDING

17   DISCLOSURES

18   None.

19   SUPPLEMENTAL MATERIAL

20   Expanded Methods

21   Expanded Results

22   Supplemental Figures I-XI

23   Supplemental Excel Tables I-IV

24   Supplemental Tables V-VI

25   References 51-75

26

REFERENCES

1. Lev M. Pathologic anatomy and interrelationship of hypoplasia of the aortic tract complexes. *Lab Invest*. 1952;1:61-70.

2. Noonan JA, Nadas AS. The hypoplastic left heart syndrome; an analysis of 101 cases. *Pediatr Clin North Am*. 1958;5:1029-1056.

3. Anderson RH, Spicer DE, Crucean A. Clarification of the definition of hypoplastic left heart syndrome. *Nat Rev Cardiol*. 2021;10.1038/s41569-020-00500-5

4. Hinton RB, Jr., Martin LJ, Tabangin ME, Mazwi ML, Cripe LH, Benson DW. Hypoplastic left heart syndrome is heritable. *J Am Coll Cardiol*. 2007;50:1590-1595.

5. Oyen N, Poulsen G, Boyd HA, Wohlfahrt J, Jensen PK, Melbye M. Recurrence of congenital heart defects in families. *Circulation*. 2009;120:295-301.

6. Hickey EJ, Caldarone CA, McCrindle BW. Left ventricular hypoplasia: A spectrum of disease involving the left ventricular outflow tract, aortic valve, and aorta. *J Am Coll Cardiol*. 2012;59:S43-54.

7. Harh JY, Paul MH, Gallen WJ, Friedberg DZ, Kaplan S. Experimental production of hypoplastic left heart syndrome in the chick embryo. *Am J Cardiol*. 1973;31:51-56.

8. Crucean A, Alqahtani A, Barron DJ, Brawn WJ, Richardson RV, O'Sullivan J, Anderson RH, Henderson DJ, Chaudhry B. Re-evaluation of hypoplastic left heart syndrome from a developmental and morphological perspective. *Orphanet J Rare Dis*. 2017;12:138.

9. Grossfeld P, Nie S, Lin L, Wang L, Anderson RH. Hypoplastic left heart syndrome: A new paradigm for an old disease? *J Cardiovasc Dev Dis*. 2019;6

10. Liu X, Yagi H, Saeed S, Bais AS, Gabriel GC, Chen Z, Peterson KA, Li Y, Schwartz MC, Reynolds WT, et al. The complex genetics of hypoplastic left heart syndrome. *Nat Genet*. 2017;49:1152-1159.

11. Meilhac SM, Lescroart F, Blanpain C, Buckingham ME. Cardiac cell lineages that form the heart. *Cold Spring Harb Perspect Med*. 2014;4:a013888.

12. Moretti A, Caron L, Nakano A, Lam JT, Bernshausen A, Chen Y, Qyang Y, Bu L, Sasaki M, Martin-Puig S, et al. Multipotent embryonic isl1+ progenitor cells lead to cardiac, smooth muscle, and endothelial cell diversification. *Cell*. 2006;127:1151-1165.

13. Kattman SJ, Huber TL, Keller GM. Multipotent flk-1+ cardiovascular progenitor cells give rise to the cardiomyocyte, endothelial, and vascular smooth muscle lineages. *Dev Cell*. 2006;11:723-732.

14. Laugwitz KL, Moretti A, Caron L, Nakano A, Chien KR. Islet1 cardiovascular progenitors: A single source for heart lineages? *Development*. 2008;135:193-205.

15. Kodo K, Ong SG, Jahanbani F, Termglinchan V, Hirono K, InanlooRahatloo K, Ebert AD, Shukla P, Abilez OJ, Churko JM, et al. Ipsc-derived cardiomyocytes reveal abnormal tgf-beta signalling in left ventricular non-compaction cardiomyopathy. *Nat Cell Biol*. 2016;18:1031-1042.

16. Ang YS, Rivas RN, Ribeiro AJS, Srivas R, Rivera J, Stone NR, Pratt K, Mohamed TMA, Fu JD, Spencer CI, et al. Disease model of gata4 mutation reveals transcription factor cooperativity in human cardiogenesis. *Cell*. 2016;167:1734-1749 e1722.

17. Theis JL, Hrstka SC, Evans JM, O'Byrne MM, de Andrade M, O'Leary PW, Nelson TJ, Olson TM. Compound heterozygous notch1 mutations underlie impaired cardiogenesis in a patient with hypoplastic left heart syndrome. *Hum Genet*. 2015;134:1003-1011.

18. Yang C, Xu Y, Yu M, Lee D, Alharti S, Hellen N, Ahmad Shaik N, Banaganapalli B, Sheikh Ali Mohamoud H, Elango R, et al. Induced pluripotent stem cell modelling of hlhs underlines the contribution of dysfunctional notch signalling to impaired cardiogenesis. *Hum Mol Genet*. 2017;26:3031-3045.

19. Hrstka SC, Li X, Nelson TJ, Wanek Program Genetics Pipeline G. Notch1-dependent nitric oxide signaling deficiency in hypoplastic left heart syndrome revealed through patient-specific phenotypes detected in bioengineered cardiogenesis. *Stem Cells*. 2017;35:1106-1119.

20. Kobayashi J, Yoshida M, Tarui S, Hirata M, Nagai Y, Kasahara S, Naruse K, Ito H, Sano S, Oh H. Directed differentiation of patient-specific induced pluripotent stem cells identifies the transcriptional repression and epigenetic modification of nkx2-5, hand1, and notch1 in hypoplastic left heart syndrome. *PLoS ONE*. 2014;9:e102796.

21. Jiang Y, Habibollah S, Tilgner K, Collin J, Barta T, Al-Aama JY, Tesarov L, Hussain R, Trafford AW, Kirkwood G, et al. An induced pluripotent stem cell model of hypoplastic left heart syndrome (hlhs) reveals multiple expression and functional differences in hlhs-derived cardiac myocytes. *Stem Cells Transl Med*. 2014;3:416-423.

22. Pinz H, Pyle LC, Li D, Izumi K, Skraban C, Tarpinian J, Braddock SR, Telegrafi A, Monaghan KG, Zackai E, et al. De novo variants in myelin regulatory factor (myrf) as candidates of a new syndrome of cardiac and urogenital anomalies. *Am J Med Genet A*. 2018;176:969-972.

23. Qi H, Yu L, Zhou X, Wynn J, Zhao H, Guo Y, Zhu N, Kitaygorodsky A, Hernan R, Aspelund G, et al. De novo variants in congenital diaphragmatic hernia identify myrf as a new syndrome and reveal genetic overlaps with other developmental disorders. *PLoS Genet*. 2018;14:e1007822.

24. Song L, Li Y, Wang K, Zhou CJ. Cardiac neural crest and outflow tract defects in lrp6 mutant mice. *Dev Dyn*. 2010;239:200-210.

25. Wu X, Shen QT, Oristian DS, Lu CP, Zheng Q, Wang HW, Fuchs E. Skin stem cells orchestrate directional migration by regulating microtubule-acf7 connections through gsk3beta. *Cell*. 2011;144:341-352.

26. Zaidi S, Choi M, Wakimoto H, Ma L, Jiang J, Overton JD, Romano-Adesman A, Bjornson RD, Breitbart RE, Brown KK, et al. De novo mutations in histone-modifying genes in congenital heart disease. *Nature*. 2013;498:220-223.

27. Jin SC, Homsy J, Zaidi S, Lu Q, Morton S, DePalma SR, Zeng X, Qi H, Chang W, Sierant MC, et al. Contribution of rare inherited and de novo variants in 2,871 congenital heart disease probands. *Nat Genet*. 2017;49:1593-1601.

28. Sahara M, Santoro F, Sohlmer J, Zhou C, Witman N, Leung CY, Mononen M, Bylund K, Gruber P, Chien KR. Population and single-cell analysis of human cardiogenesis reveals unique lgr5 ventricular progenitors in embryonic outflow tract. *Dev Cell*. 2019;48:475-490 e477.

29. Cui Y, Zheng Y, Liu X, Yan L, Fan X, Yong J, Hu Y, Dong J, Li Q, Wu X, et al. Single-cell transcriptome analysis maps the developmental track of the human heart. *Cell Rep*. 2019;26:1934-1950 e1935.

30. Krumm N, Turner TN, Baker C, Vives L, Mohajeri K, Witherspoon K, Raja A, Coe BP, Stessman HA, He ZX, et al. Excess of rare, inherited truncating mutations in autism. *Nat Genet*. 2015;47:582-588.

31. Bergmann O, Zdunek S, Felker A, Salehpour M, Alkass K, Bernard S, Sjostrom SL, Szewczykowska M, Jackowska T, Dos Remedios C, et al. Dynamics of cell generation and turnover in the human heart. *Cell*. 2015;161:1566-1575.

32. Cao N, Liang H, Huang J, Wang J, Chen Y, Chen Z, Yang HT. Highly efficient induction and long-term maintenance of multipotent cardiovascular progenitors from human pluripotent stem cells under defined conditions. *Cell Res*. 2013;23:1119-1132.

33. Burridge PW, Matsa E, Shukla P, Lin ZC, Churko JM, Ebert AD, Lan F, Diecke S, Huber B, Mordwinkin NM, et al. Chemically defined generation of human cardiomyocytes. *Nat Methods*. 2014;11:855-860.

34. Hatcher CJ, Kim MS, Mah CS, Goldstein MM, Wong B, Mikawa T, Basson CT. Tbx5 transcription factor regulates cell proliferation during cardiogenesis. *Dev Biol*. 2001;230:177-188.

35. Mathiassen SG, De Zio D, Cecconi F. Autophagy and the cell cycle: A complex landscape. *Front Oncol*. 2017;7:51.

36. Klausner RD, Donaldson JG, Lippincott-Schwartz J. Brefeldin a: Insights into the control of membrane traffic and organelle structure. *J Cell Biol*. 1992;116:1071-1080.

37. Xu H, Tsang KS, Wang Y, Chan JC, Xu G, Gao WQ. Unfolded protein response is required for the definitive endodermal specification of mouse embryonic stem cells via smad2 and beta-catenin signaling. *J Biol Chem*. 2014;289:26290-26301.

38. Laguesse S, Creppe C, Nedialkova DD, Prevot PP, Borgs L, Huysseune S, Franco B, Duysens G, Krusy N, Lee G, et al. A dynamic unfolded protein response contributes to the control of cortical neurogenesis. *Dev Cell*. 2015;35:553-567.

39. Mao C, Tai WC, Bai Y, Poizat C, Lee AS. In vivo regulation of grp78/bip transcription in the embryonic heart: Role of the endoplasmic reticulum stress response element and gata-4. *J Biol Chem*. 2006;281:8877-8887.

40. Hetz C. The unfolded protein response: Controlling cell fate decisions under er stress and beyond. *Nat Rev Mol Cell Biol*. 2012;13:89-102.

41. Li G, Tian L, Goodyer W, Kort EJ, Buikema JW, Xu A, Wu JC, Jovinge S, Wu SM. Single cell expression analysis reveals anatomical and cell cycle-dependent transcriptional shifts during heart development. *Development*. 2019;146

42. Jia G, Preussner J, Chen X, Guenther S, Yuan X, Yekelchyk M, Kuenne C, Looso M, Zhou Y, Teichmann S, et al. Single cell rna-seq and atac-seq analysis of cardiac progenitor cell transition states and lineage settlement. *Nat Commun*. 2018;9:4877.

43. Asp M, Giacomello S, Larsson L, Wu C, Furth D, Qian X, Wardell E, Custodio J, Reimegard J, Salmen F, et al. A spatiotemporal organ-wide gene expression and cell atlas of the developing human heart. *Cell*. 2019;179:1647-1660 e1619.

44. Guo H, Tian L, Zhang JZ, Kitani T, Paik DT, Lee WH, Wu JC. Single-cell rna sequencing of human embryonic stem cell differentiation delineates adverse effects of nicotine on embryonic development. *Stem Cell Reports*. 2019;12:772-786.

45. Fischer C, Milting H, Fein E, Reiser E, Lu K, Seidel T, Schinner C, Schwarzmayr T, Schramm R, Tomasi R, et al. Long-term functional and structural preservation of precision-cut human myocardium under continuous electromechanical stimulation in vitro. *Nat Commun*. 2019;10:117.

46. Lakin ND, Jackson SP. Regulation of p53 in response to DNA damage. *Oncogene*. 1999;18:7644-7655.

47. Foglia MJ, Poss KD. Building and re-building the heart by cardiomyocyte proliferation. *Development*. 2016;143:729-740.

48. Miao Y, Tian L, Martin M, Paige SL, Galdos FX, Li J, Klein A, Zhang H, Ma N, Wei Y, et al. Intrinsic endocardial defects contribute to hypoplastic left heart syndrome. *Cell Stem Cell*. 2020;10.1016/j.stem.2020.07.015

49. Gaber N, Gagliardi M, Patel P, Kinnear C, Zhang C, Chitayat D, Shannon P, Jaeggi E, Tabori U, Keller G, et al. Fetal reprogramming and senescence in hypoplastic left heart syndrome and in human pluripotent stem cells during cardiac differentiation. *Am J Pathol*. 2013;183:720-734.

50. Freud LR, McElhinney DB, Marshall AC, Marx GR, Friedman KG, del Nido PJ, Emani SM, Lafranchi T, Silva V, Wilkins-Haug LE, et al. Fetal aortic valvuloplasty for evolving hypoplastic left heart syndrome: Postnatal outcomes of the first 100 patients. *Circulation*. 2014;130:638-645.

**References related to Supplemental Methods and Results**

51. Gramlich M, Pane LS, Zhou Q, Chen Z, Murgia M, Schotterl S, Goedel A, Metzger K, Brade T, Parrotta E, et al. Antisense-mediated exon skipping: A therapeutic strategy for titin-based dilated cardiomyopathy. *EMBO Mol Med*. 2015;10.15252/emmm.201505047

52. Moretti A, Fonteyne L, Giesert F, Hoppmann P, Meier AB, Bozoglu T, Baehr A, Schneider CM, Sinnecker D, Klett K, et al. Somatic gene editing ameliorates skeletal and cardiac muscle failure in pig and human models of duchenne muscular dystrophy. *Nat Med*. 2020;26:207-214.

53. Moretti A, Bellin M, Welling A, Jung CB, Lam JT, Bott-Flugel L, Dorn T, Goedel A, Hohnke C, Hofmann F, et al. Patient-specific induced pluripotent stem-cell models for long-qt syndrome. *N Engl J Med*. 2010;363:1397-1409.

54. Burridge PW, Holmstrom A, Wu JC. Chemically defined culture and cardiomyocyte differentiation of human pluripotent stem cells. *Curr Protoc Hum Genet*. 2015;87:21 23 21-15.

55. Dorn T, Kornherr J, Parrotta EI, Zawada D, Ayetey H, Santamaria G, Iop L, Mastantuono E, Sinnecker D, Goedel A, et al. Interplay of cell-cell contacts and rhoa/mrtf-a signaling regulates cardiomyocyte identity. *EMBO J*. 2018;37

56. Gilsbach R, Schwaderer M, Preissl S, Gruning BA, Kranzhofer D, Schneider P, Nuhrenberg TG, Mulero-Navarro S, Weichenhan D, Braun C, et al. Distinct epigenetic programs regulate cardiac myocyte development and disease in the human heart in vivo. *Nat Commun*. 2018;9:391.

57. Takata A, Ionita-Laza I, Gogos JA, Xu B, Karayiorgou M. De novo synonymous mutations in regulatory elements contribute to the genetic etiology of autism and schizophrenia. *Neuron*. 2016;89:940-947.

58. Cerami E, Demir E, Schultz N, Taylor BS, Sander C. Automated network analysis identifies core pathways in glioblastoma. *PLoS ONE*. 2010;5:e8918.

59. Futschik ME, Carlisle B. Noise-robust soft clustering of gene expression time-course data. *J Bioinform Comput Biol*. 2005;3:965-988.

60. Shannon P, Markiel A, Ozier O, Baliga NS, Wang JT, Ramage D, Amin N, Schwikowski B, Ideker T. Cytoscape: A software environment for integrated models of biomolecular interaction networks. *Genome Res*. 2003;13:2498-2504.

61. Satija R, Farrell JA, Gennert D, Schier AF, Regev A. Spatial reconstruction of single-cell gene expression data. *Nat Biotechnol*. 2015;33:495-502.

62. Chen J, Bardes EE, Aronow BJ, Jegga AG. Toppgene suite for gene list enrichment analysis and candidate gene prioritization. *Nucleic Acids Res*. 2009;37:W305-311.

63. Trapnell C, Cacchiarelli D, Grimsby J, Pokharel P, Li S, Morse M, Lennon NJ, Livak KJ, Mikkelsen TS, Rinn JL. The dynamics and regulators of cell fate decisions are revealed by pseudotemporal ordering of single cells. *Nat Biotechnol*. 2014;32:381-386.

64. Churko JM, Garg P, Treutlein B, Venkatasubramanian M, Wu H, Lee J, Wessells QN, Chen SY, Chen WY, Chetal K, et al. Defining human cardiac transcription factor hierarchies using integrated single-cell heterogeneity analysis. *Nat Commun*. 2018;9:4906.

65. Tirosh I, Venteicher AS, Hebert C, Escalante LE, Patel AP, Yizhak K, Fisher JM, Rodman C, Mount C, Filbin MG, et al. Single-cell rna-seq supports a developmental hierarchy in human oligodendroglioma. *Nature*. 2016;539:309-313.

66. DeLaughter DM, Bick AG, Wakimoto H, McKean D, Gorham JM, Kathiriya IS, Hinson JT, Homsy J, Gray J, Pu W, et al. Single-cell resolution of temporal gene expression during heart development. *Dev Cell*. 2016;39:480-490.

67. Kulak NA, Pichler G, Paron I, Nagaraj N, Mann M. Minimal, encapsulated proteomic-sample processing applied to copy-number estimation in eukaryotic cells. *Nat Methods*. 2014;11:319-324.

68. Scheltema RA, Hauschild JP, Lange O, Hornburg D, Denisov E, Damoc E, Kuehn A, Makarov A, Mann M. The q exactive hf, a benchtop mass spectrometer with a pre-filter, high-performance quadrupole and an ultra-high-field orbitrap analyzer. *Mol Cell Proteomics*. 2014;13:3698-3708.

69. Kelstrup CD, Jersie-Christensen RR, Batth TS, Arrey TN, Kuehn A, Kellmann M, Olsen JV. Rapid and deep proteomes by faster sequencing on a benchtop quadrupole ultra-high-field orbitrap mass spectrometer. *J Proteome Res*. 2014;13:6187-6195.

70. Cox J, Mann M. Maxquant enables high peptide identification rates, individualized p.P.B.-range mass accuracies and proteome-wide protein quantification. *Nat Biotechnol*. 2008;26:1367-1372.

71. International Stem Cell I, Amps K, Andrews PW, Anyfantis G, Armstrong L, Avery S, Baharvand H, Baker J, Baker D, Munoz MB, et al. Screening ethnically diverse human embryonic stem cells identifies a chromosome 20 minimal amplicon conferring growth advantage. *Nat Biotechnol*. 2011;29:1132-1144.

72. Taapken SM, Nisler BS, Newton MA, Sampsell-Barron TL, Leonhard KA, McIntire EM, Montgomery KD. Karotypic abnormalities in human induced pluripotent stem cells and embryonic stem cells. *Nat Biotechnol*. 2011;29:313-314.

73. Chan LL, Shen D, Wilkinson AR, Patton W, Lai N, Chan E, Kuksin D, Lin B, Qiu J. A novel image-based cytometry method for autophagy detection in living cells. *Autophagy*. 2012;8:1371-1382.

74. Dagda RK, Zhu J, Kulich SM, Chu CT. Mitochondrially localized erk2 regulates mitophagy and autophagic cell stress: Implications for parkinson's disease. *Autophagy*. 2008;4:770-782.

75. Chu CT, Plowey ED, Dagda RK, Hickey RW, Cherra SJ, 3rd, Clark RS. Autophagy in neurite injury and neurodegeneration: In vitro and in vivo models. *Methods Enzymol*. 2009;453:217-249.

1

2
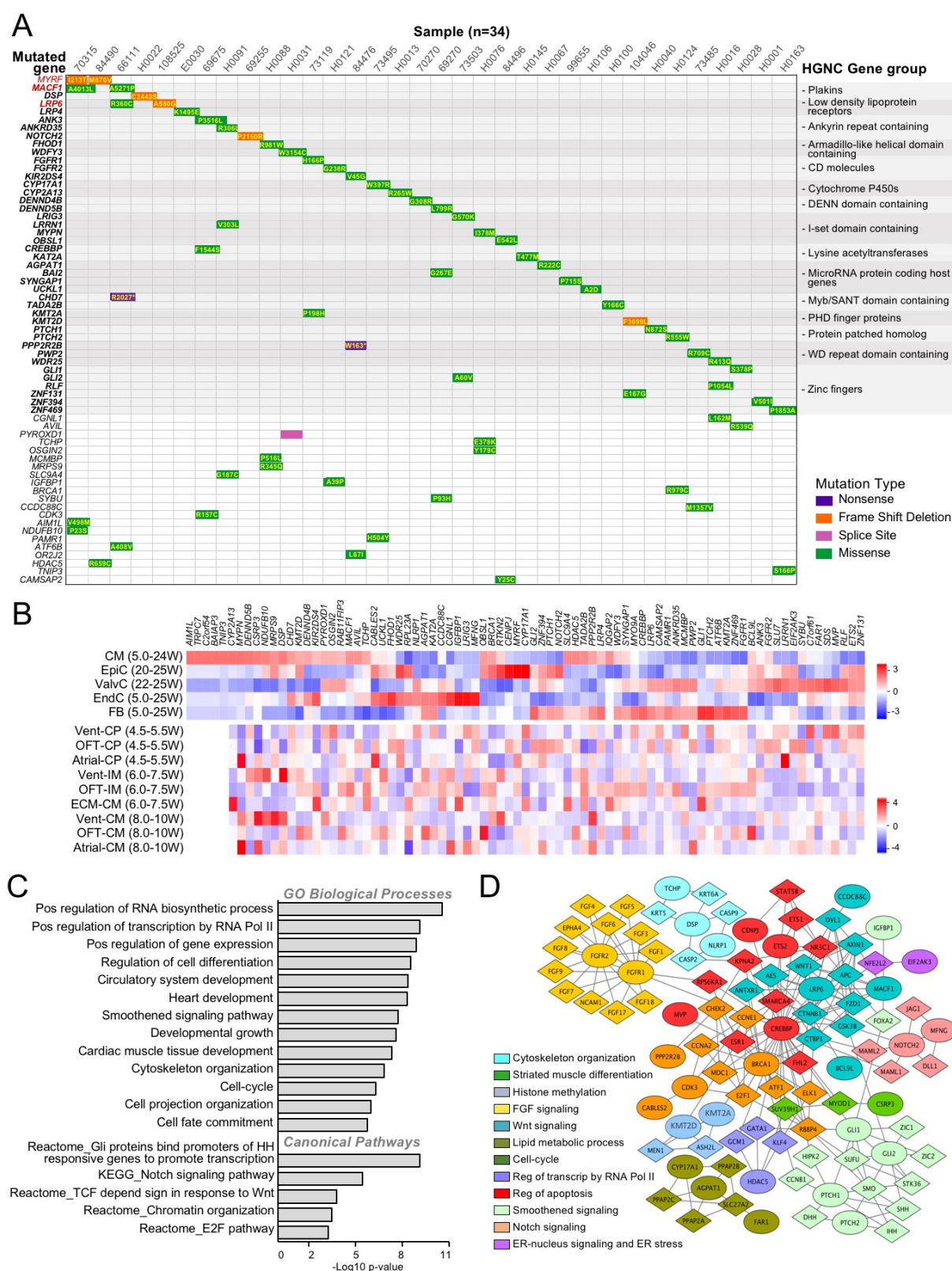
3 **Figure 1. Characterization of D-DNMs in HLHS patients. A**, Waterfall plot of de-novo

4 multihit genes (red) or gene family (bold) identified in the HLHS cohort. Additional de-novo

5 genes in each subject are in plain black. **B**, Cell type-specific expression of HLHS D-DNM

1   genes based on scRNA-seq from normal fetal hearts between 4.5 and 25 weeks (W) of

2   gestation. Data from Ciu et al.[29] and Sahara et al.[28] were used to generate the upper and

3   lower heatmap, respectively. ECM, extracellular matrix; EndC, endothelial cells; EpiC,

4   epicardial cells; FB, fibroblasts; IM, intermediates; ValvC; valvular cells; Vent, ventricular. **C**

5   and **D**, Bar chart of Gene Ontology (GO) enrichment analysis (C) and protein-protein network

6   analysis (D) of D-DNM genes. In D, each Netbox module is coded by a different color, with

7   mutated genes illustrated as circle and linker genes as diamonds.
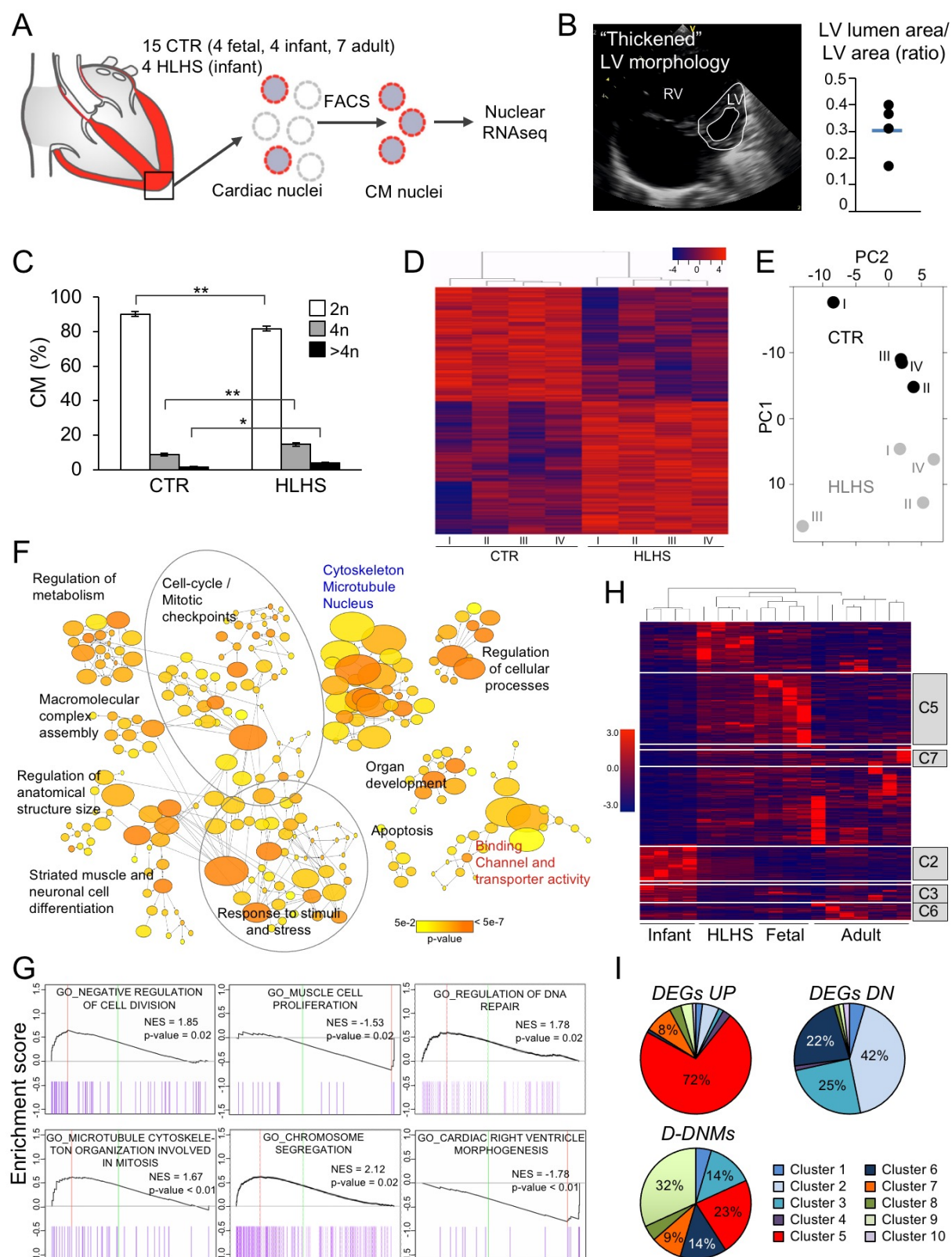
Figure 2. Gene expression analysis of CM nuclei from HLHS and control hearts. A, Workflow of CM nuclei isolation for RNAseq. **B**, Representative echocardiogram of HLHS patients with a distinct LV phenotype. Dot plot shows the ratio of LV lumen area/LV area for

33

1   the 4 HLHS patients and the average value (blue line). **C**, Ploidy level of CM nuclei in HLHS

2   and control (CTR) hearts. Data are mean ± SEM. *p<0.05, **p<0.01 (t test). **D**, Heatmap

3   depicting normalized RNAseq expression values of DEGs (1.5-fold-expression, *p*-value

4   ≤0.05). Gene regulations are reported as a color code and hierarchical clustering result as a

5   dendrogram. **E**, PCA performed on rlog-normalized (DESeq2) counts for all nuclear RNAseq

6   samples. **F**, Network visualization of the enriched GOs of HLHS DEGs using the Cytoscape

7   plugins BinGO. Nodes represent enriched GO terms, node size corresponds to the gene

8   number and color intensity to the *p*-value. Edges represent GO relation of Biological Process

9   (black), Molecular Function (red), and Cellular Component (blue). **G**, Representative GSEA

10   enrichment plots. Normalized enrichment score (NES) and *p*-value are specified. **H**,

11   Heatmap illustrating the expression of HLHS DEGs during fetal, infant, and adult stages of

12   normal cardiac development. The dendrogram shows clustering of the HLHS infant samples

13   with control fetal samples. Genes belonging to developmentally regulated gene clusters from

14   Figure IIIC in the Data Supplement are highlighted. **I**, Pie charts showing the percentage of

15   HLHS upregulated (DEGs UP), downregulated (DEGs DN), and damaging *de-novo* affected

16   (D-DNM) genes belonging to the developmentally regulated gene clusters from Figure IIIC in

17   the Data Supplement.
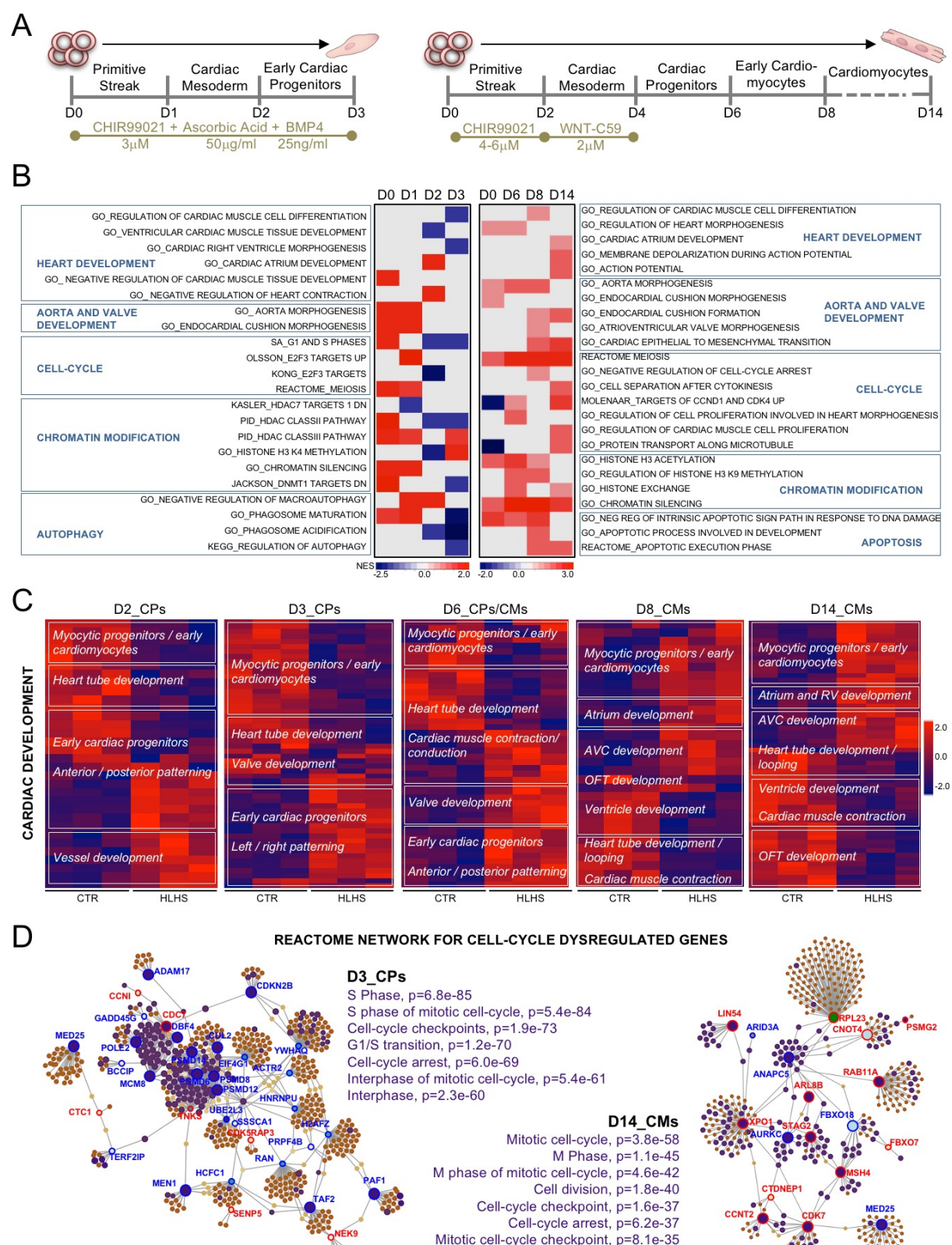
Figure 3. Gene expression analysis during iPSC-based cardiogenesis reveals networks of dysregulated genes in HLHS. A, Directed iPSC cardiac differentiation protocols used in the study. **B**, Heatmap of normalized enrichment scores (NES) for selected

35

1   GSEA terms. Red and blue denotes terms with positive and negative NES, respectively. **C**,

2   Heatmaps showing gene expression of DEGs (1.5-fold-expression, *p*-value ≤0.05) involved

3   in cardiac development at the indicated days of differentiation. Values are row-scaled to

4   show their relative expression. Blue and red are low and high levels respectively. **D**,

5   Networkanalyst-generated protein-protein interactome of DEGs involved in cell-cycle at D3

6   and D14. Upregulated (red) and downregulated (blue) genes are shown. In purple are

7   highlighted the genes belonging to the enriched GO categories specified on the side of the

8   plots. Protein–protein interactions are indicated as solid gray lines between genes.
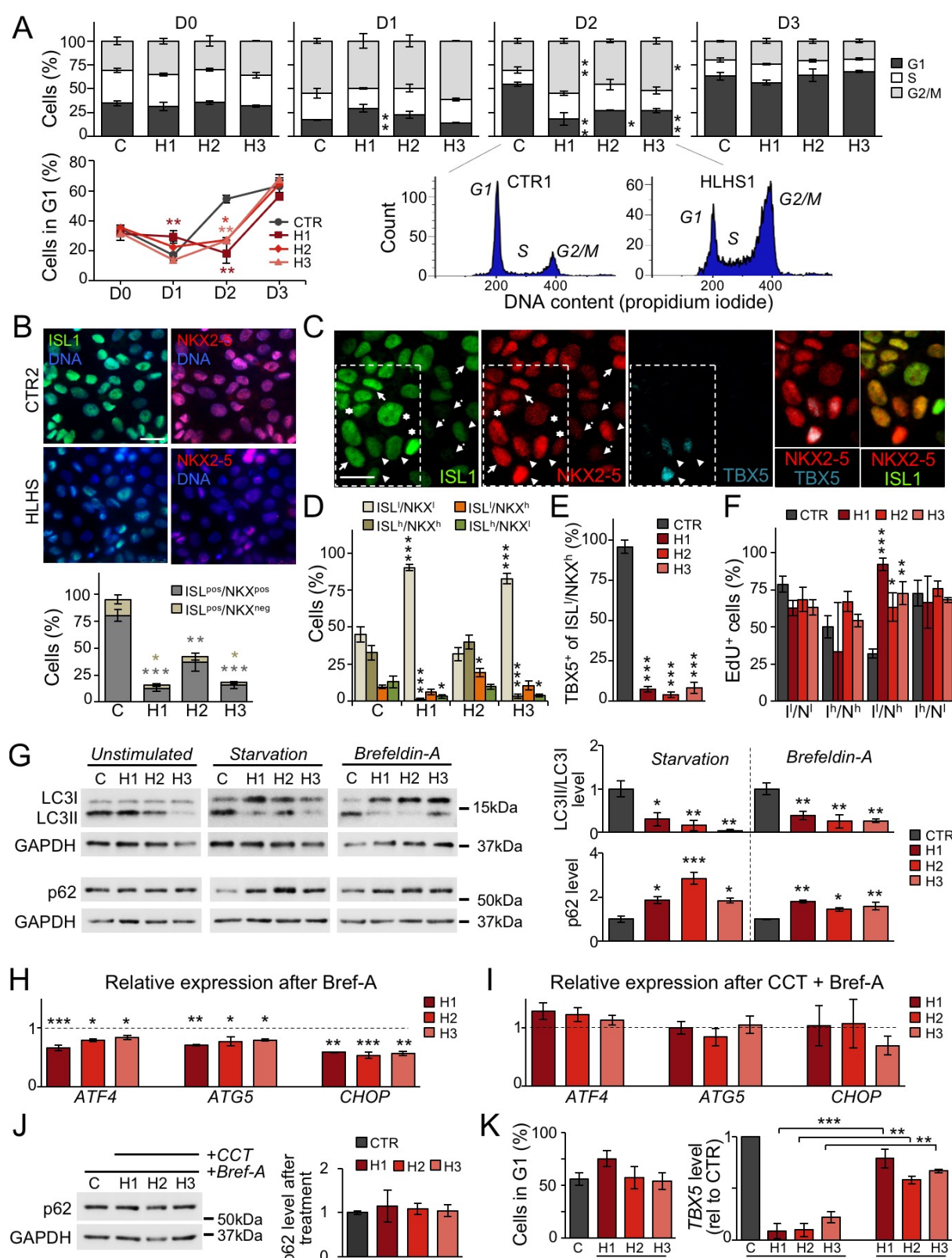
Figure 4. Defects in UPR and autophagy delay and disrupt CP lineage specification. To better discriminate possible phenotypic variations among diseased lines, functional results from each HLHS line are shown separately. Data from control lines have been combined. **A**,

1　　Propidium iodide staining analysis of HLHS (H) and control cells (C) during CP

2　　differentiation. Data are mean ± SEM, n=2-4 differentiations per line, N≥20000 cells per

3　　sample at each time point. *p<0.05, **p<0.01 compared to CTR (two-way ANOVA). **B**,

4　　Immunofluorescence analysis of ISL1 and NKX2-5 in HLHS and control CPs at D2. Scale

5　　bar, 25 μm. Data are mean ± SEM, 431 (CTR), 463 (HLHS1), 442 (HLHS2) and 396

6　　(HLHS3) cells from n=3 differentiations per line. *p<0.05, **p<0.01, ***p<0.001 compared to

7　　CTR (one-way ANOVA). **C**, Representative immunofluorescence of ISL1, NKX2-5 and TBX5

8　　in control CPs (CTR3) at D3. Four ISL1/NKX2-5 expression patterns are highlighted:

9　　ISL1^{low}/NKX2-5^{low}　(dotted　arrows),　ISL1^{high}/NKX2-5^{high}　(arrows),　ISL1^{high}/NKX2-5^{low}

10　　(asterisks), and ISL1^{low}/NKX2-5^{high} (arrow heads). Scale bar, 20 μm. **D**, Distribution of cells

11　　with ISL1/NKX2-5 expression patterns from (C) in HLHS and control CPs at D3. Data are

12　　mean ± SEM, 369 (CTR), 347 (HLHS1), 322 (HLHS2), 357 (HLHS3) cells from 3

13　　differentiations per line. *p<0.05, ***p<0.001 compared to CTR (one-way ANOVA). **E**,

14　　Percentage of ISL1^{low}/NKX2-5^{high} cells expressing TBX5 in HLHS and control CPs at D3.

15　　Data are mean ± SEM, 114 (CTR), 70 (HLHS1), 182 (HLHS2) and 123 (HLHS3) cells from

16　　n=3 differentiations per line. ***p<0.001 compared to CTR (one-way ANOVA). **F**,

17　　Quantification of EdU$^+$ cells in HLHS and control CP subpopulations at D3. Data are mean ±

18　　SEM, 369 (CTR), 347 (HLHS1), 322 (HLHS2), 357 (HLHS3) cells from 3 differentiations per

19　　line. *p<0.05, **p<0.005, ***p<0.001 compared to CTR (one-way ANOVA). **G**, Western blot

20　　of LC3 and p62 in HLHS and control CPs at D3 with and without starvation or brefeldin-A.

21　　For detection of LC3, all three conditions were carried out in presence of chloroquine. Data

22　　are mean ± SEM, n=2-3 differentiations per line. *p<0.05, **p<0.01, ***p<0.001 compared to

23　　CTR (one-way ANOVA). **H** and **I**, Expression analysis of *ATF4* and its downstream targets

24　　*ATG5* and *CHOP* in HLHS and control CPs at D3 after treatment with brefeldin-A alone (H)

25　　or in combination with the PERK activator CCT020312 (I). Shown are expression levels

26　　relative to controls. Data are mean ± SEM, n=2-4 differentiations per line. *p<0.05, **p<0.01,

27　　***p<0.001 compared to CTR (one-way ANOVA). **J**, Western blot of p62 in HLHS and control

28　　CPs at D3 after treatment with brefeldin-A and CCT020312. Data are mean ± SEM, n=3-6

1   differentiations per line. **K**, Propidium iodide staining-based quantification of cells in G1

2   phase in HLHS and control CPs at D2 (left) and *TBX5* expression by qRT-PCR at D3 (right)

3   after 6h-treatment of HLHS cells with CCT020312 at D1.5. Data are mean ± SEM, n=2-3

4   differentiations per line, N≥20000 cells per sample in left panel. **p<0.01, ***p<0.001

5   compared to own basal (one-way ANOVA).
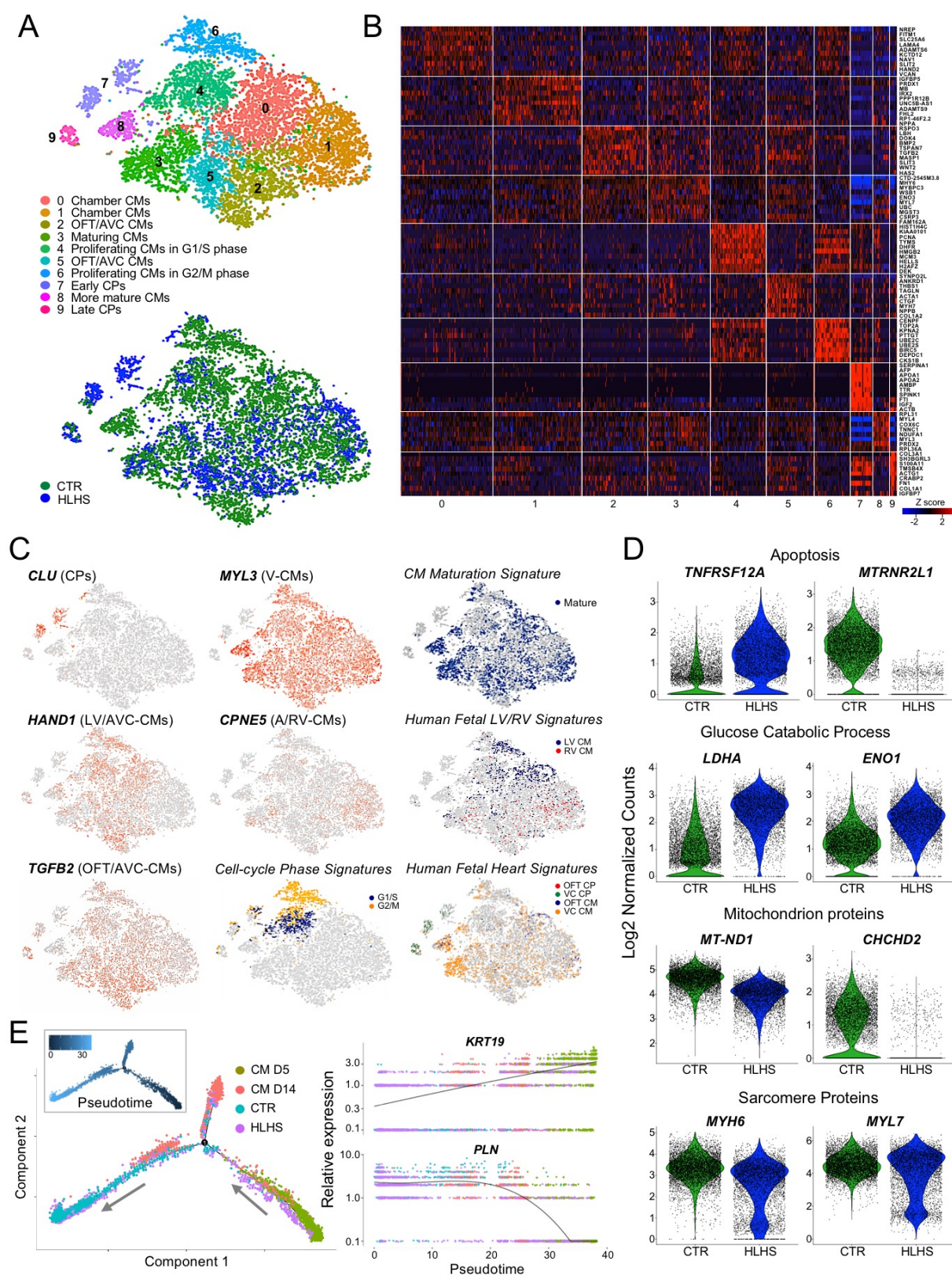
Figure 5. Single-cell RNAseq of iPSC-CMs reveals defects in cardiac lineage segregation and maturation in HLHS. A, t-SNE plot of all HLHS and CTR cell populations captured at D14 colored by cluster identity (top) and genotype (bottom). Data are from 2

1   control (CTR2 and CTR3) and 2 HLHS (HLHS2 and HLHS3) lines. **B**, Heatmap showing Z

2   score scaled average expression levels of the top ten DEGs for each cellular cluster. **C**,

3   Expression of selected genes marking subpopulations on t-SNE plot. Single gene panels: red

4   and gray indicates high and low expression, respectively. Signature panels: color key

5   indicates cells matching with the gene signatures tested (see Expanded Methods). A, atria;

6   VC, ventricular chamber. **D**, Violin plots of selected DEGs between CTR and HLHS cells. All

7   genes represented have a *p*-value <0.05. **E**, Branching analysis of HLHS and CTR CMs at

8   D14 together with CMs at D5 and D14 from[44] colored by genotype and estimated pseudotime

9   along the inferred cell trajectory (inset). Pseudotime dynamics of early (*KRT19*) and mature

10   (*PLN*) CM genes in dependence on inferred cell identity.

1

2
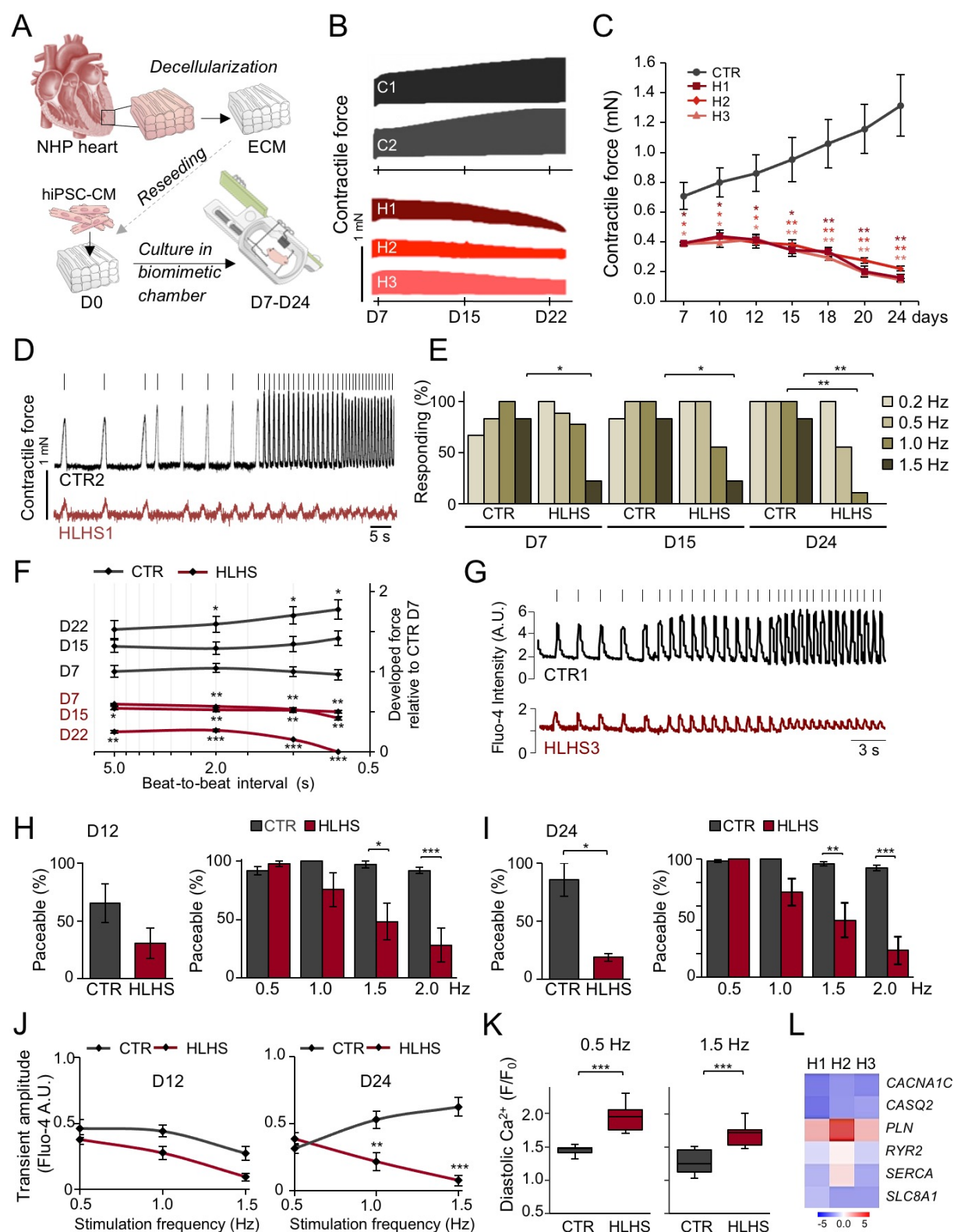
3 **Figure 6. Three-dimensional culture of iPSC-CMs under electromechanical stress**

4 **reveals HLHS-related functional abnormalities. A**, Schematic of the experimental setup

5 for 3D culture of iPSC-CMs within decellularized heart patches kept in biomimetic chambers

42

1   providing mechanical load and electrical stimulation while allowing continuous monitoring of

2   force development. All measurements were done in patches generated from 2 control and 3

3   HLHS lines. Unless otherwise illustrated, results from different control and HLHS lines have

4   been pooled. NHP, non-human primate. **B** and **C**, Representative plots (B) and statistical

5   analysis (C) of contractile force in HLHS and control patches over 24 days of culture. In (C),

6   data are mean ± SEM of serial measurements at the indicated days, n=8 (CTR), n=3 (HLHS1

7   and HLHS2), n=6 (HLHS3) patches. *p<0.05, **p<0.01 compared to CTR (two-way repeated-

8   measures ANOVA). **D**, Representative traces of contraction force at increasing stimulation

9   frequencies in one control and one HLHS line from an experiment aimed at assessing the

10 force-frequency relationship and the paceability at different stimulation frequencies.

11 Stimulation pulses are indicated as vertical bars above the respective tracing. **E**, Percentage

12 of patches responding to stimulation at indicated pacing frequencies. n=6 (CTR) and n=9

13 (HLHS). *p<0.05, **p<0.01 compared to CTR at the same day and frequency (Fisher's exact

14 test). **F**, Force-frequency relationship (FFR), depicted as the developed force (normalized to

15 the mean force developed by CTR patches at day 7) as a function of the beat-to-beat interval

16 (depicted on a logarithmic scale). Serial FFR values obtained from HLHS (n=11) and control

17 (n=8) patches at indicated time points are shown. Data are mean ± SEM. *p<0.05, **p<0.01,

18 ***p<0.001 compared to CTR at D7 at the same beat-to-beat interval (mixed effects model).

19 **G**, Representative images of Fluo-4-based intracellular calcium transients from single control

20 and HLHS CMs within the patch at increasing pacing rates. Vertical bars over the tracings

21 represent the stimulation pulses. **H** and **I**, The left graph shows the overall percentage of

22 paceable CMs within control and HLHS patches at D12 (H) and D24 (I) of 3D culture. The

23 right graph shows, only considering cells that were paceable with at least one of the applied

24 pacing rates, the percentage of cells responding at the indicated frequencies at D12 (H) and

25 D24 (I). Data are mean ± SEM, n=6 (CTR) and n=9 (HLHS) patches; left panels: N=183 and

26 156 (CTR), N=466 and 70 (HLHS) cells in (H) and (I), respectively; right panels: N≥67 and 90

27 (CTR), N≥21 and 17 (HLHS) cells for each frequency in (H) and (I), respectively. *p<0.05,

28 **p<0.01, ***p<0.001 compared to CTR (Mann Whitney test for left panels and two-way

43

1   ANOVA for right panels). **J**, Amplitude of the systolic calcium transients plotted as a function

2   of the stimulation frequency for CMs within control (n=6) and HLHS (n=9) patches at D12

3   and D24 of 3D culture. N≥65 and 81 (CTR), N≥3 and 35 (HLHS) cells for each frequency at

4   D12 and D24, respectively. Data are mean ± SEM. **p<0.01, ***p<0.001 compared to CTR

5   (two-way ANOVA). **K**, Diastolic calcium level (expressed as ratio of the diastolic Fluo-4

6   intensity at the indicated pacing frequency (*F*) and the basal Fluo-4 intensity at the beginning

7   of the experiment (F_0)) of single CMs in D24 control (n=6) and HLHS (n=9) patches at 0.5 Hz

8   and 1.5 Hz pacing rates. N=91 and 83 (CTR), N=70 and 44 (HLHS) cells at 0.5 Hz and 1.5

9   Hz, respectively. Data are mean ± SEM. ***p<0.001 (Mann Whitney test). **L**, Expression level

10   of key genes for electromechanical coupling (black) and Ca^{2+} homeostasis (red) in CMs

11   isolated from HLHS and control 3D patches at D12. Data are log2 mean fold changes

12   relative to controls, n=3 patches per line.
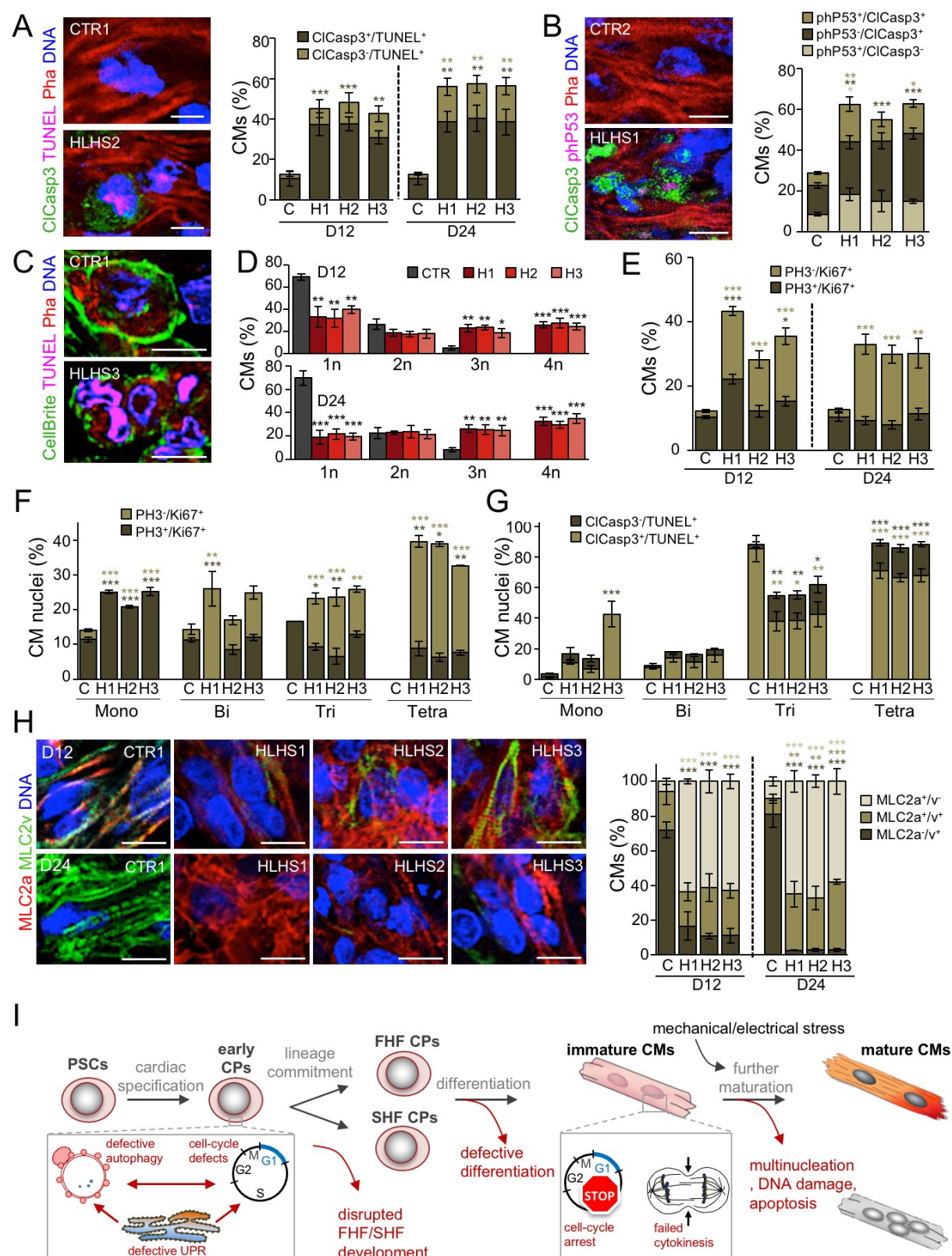
Figure 7. Aberrant apoptosis, multinucleation, and maturation of HLHS CMs in 3D biomimetic culture. All measurements were done in patches generated from 2 control and 3 HLHS lines. Results from the 2 different controls have been pooled. **A**, Representative

45

1   fluorescence images of D24 control and HLHS patches after immunostaining for activated

2   caspase 3 (ClCasp3) in conjunction with TUNEL labeling. Phalloidin (Pha) marks F-actin

3   and distinguishes CMs. Scale bar, 10 µm. Bar graph shows the statistical evaluation of D12

4   and D24. Data are mean ± SEM, n=8 (CTR, N=226 cells) and n=4 (each HLHS line, N≥200

5   cells per line) patches at D12; n=7 (CTR, N=534) and n=3 (each HLHS line, N≥434 cells per

6   line) patches at D24. **$p < 0.01$, ***$p < 0.001$ compared to CTR (one-way ANOVA). **B**,

7   Representative immunostaining for activated Caspase 3 (ClCasp3) and phosphorylated P53

8   (phP53) in D24 control and HLHS patches. Scale bar, 10 µm. Bar graph illustrates the

9   percentages of CMs (identified by Pha) expressing one or both markers. Data are mean ±

10   SEM, n=10 (CTR, N=652 cells), n=6 (HLHS1, N=572 cells), n=5 (HLHS2, N=470 cells), and

11   n=5 (HLHS3, N=314 cells) patches. *$p < 0.05$, **$p < 0.01$, ***$p < 0.001$ compared to CTR (one-

12   way ANOVA). **C**, Representative fluorescence images of CMs (identified by Pha) after

13   plasmamembrane (CellBrite), TUNEL, and DNA labeling within control and HLHS patches at

14   D24. Scale bar, 10 µm. **D**, Bar graphs showing the percentage of CMs with one (1n), two

15   (2n), three (3n) and four (4n) nuclei in the different cell lines at D12 and D24. Data are mean

16   ± SEM, n=6 (CTR, N=340 cells) and n=3 (each HLHS line, N≥182 cells per line) patches at

17   D12; n=6 (CTR, N=341) and n=3 (each HLHS line, N≥147 cells per line) patches at D24.

18   *$p < 0.05$, **$p < 0.01$, ***$p < 0.001$ compared to CTR (one-way ANOVA). **E**, Bar graphs showing

19   the percentage of CMs positive for phosphorylated histone 3 (PH3) and Ki67 at D12 and

20   D24. Data are mean ± SEM, n=7 (CTR, N=528 cells), and n=7 (HLHS1, N=698 cells), n=5

21   (HLHS2, N=463), and n=5 (HLHS3, N=668) patches at D12; n=7 (CTR, N=673 cells), and

22   n=7 (HLHS1, N=682 cells), n=5 (HLHS2, N=486), and n=5 (HLHS3, N=485) patches at D24.

23   *$p < 0.05$, **$p < 0.01$, ***$p < 0.001$ compared to CTR (one-way ANOVA). **F,** Bar graph showing

24   the percentage of nuclei positive for PH3 and Ki67 in mono-, bi-, tri-, and tetra-nucleated

25   CMs at D24. Data are mean ± SEM, n=3 patches per line; N=331 (CTR), N=258 (HLHS1),

26   N=228 (HLHS2), and N=240 (HLHS3) cells. *$p < 0.05$, **$p < 0.01$, ***$p < 0.001$ compared to CTR

27   (one-way ANOVA). **G**, Bar graph showing the percentage of nuclei positive for ClCasp3 and

28   phP53 in mono-, bi-, tri-, and tetra-nucleated CMs at D24. Data are mean ± SEM, Data are

46

1   mean ± SEM, n=7 (CTR) and n=3 (each HLHS line) patches; N=401 (CTR), N=194 (HLHS1),

2   N=175 (HLHS2), and N=237 (HLHS3) cells. *p<0.05, **p<0.01, ***p<0.001 compared to CTR

3   (one-way ANOVA). **H**, Left, representative immunostains for MLC2a and MLC2v in control

4   and HLHS patches. Scale bar, 10 μm. Right, bar graph shows statistical evaluation. Data are

5   mean ± SEM, n=8 (CTR, N=951 cells) and n=4 (each HLHS line, N≥428 cells per line)

6   patches at D12; n=8 (CTR, N=949) and n=4 (each HLHS line, N≥442 cells per line) patches

7   at D24. **p<0.01, ***p<0.001 compared to CTR (one-way ANOVA). **I**, Scheme depicting the

8   identified steps during cardiac development at which HLHS-related abnormalities interfere

9   with normal development and contribute to the complex CHD phenotype.